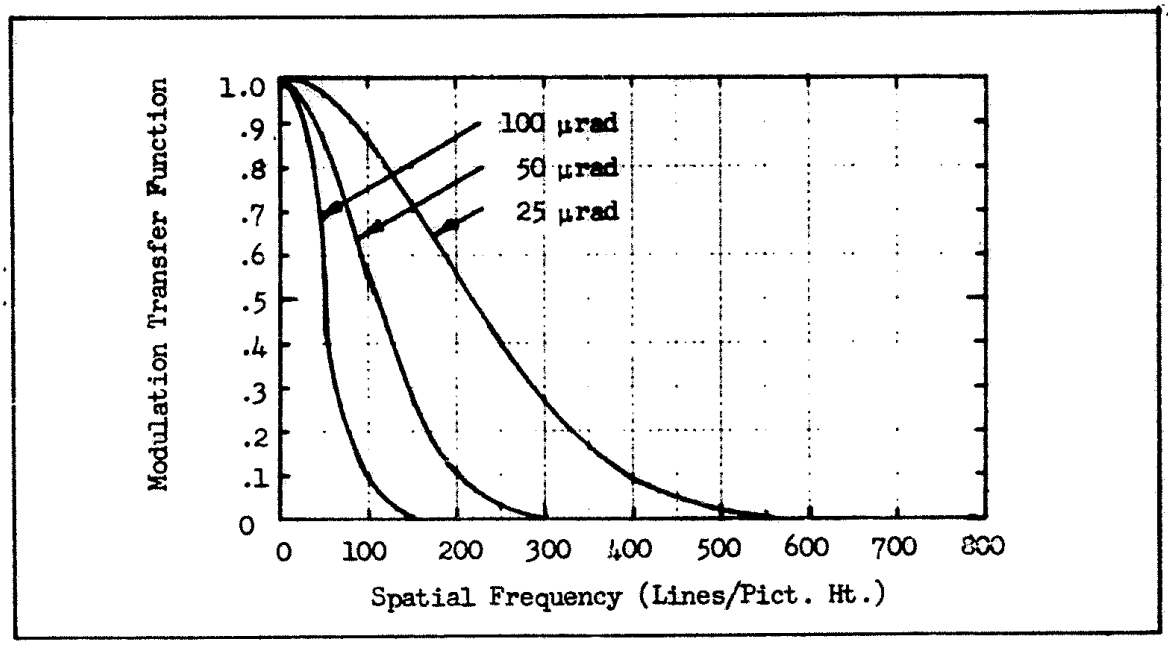

Fig. 34 Modulation Transfer Function for the Assumed System with Random Image Motion of RMS Amplitude 25, 50 and 100 microradians per Exposure Time.

lines per picture height.

By analogy to the sinusoidal motion case, we can write

$$\Delta\theta_c = \frac{\Delta\theta_v}{0.89} \quad , \tag{49}$$

and

$$N_c = \frac{0.89Y}{F_L \bullet \Delta\theta_v} \quad , \tag{50}$$

which are plotted in Fig. 35. The MTF normalized to the cut-off frequency is given by

$$R_o(N) = e^{-3.92(\frac{N}{N_c})^2} \quad , \tag{51}$$

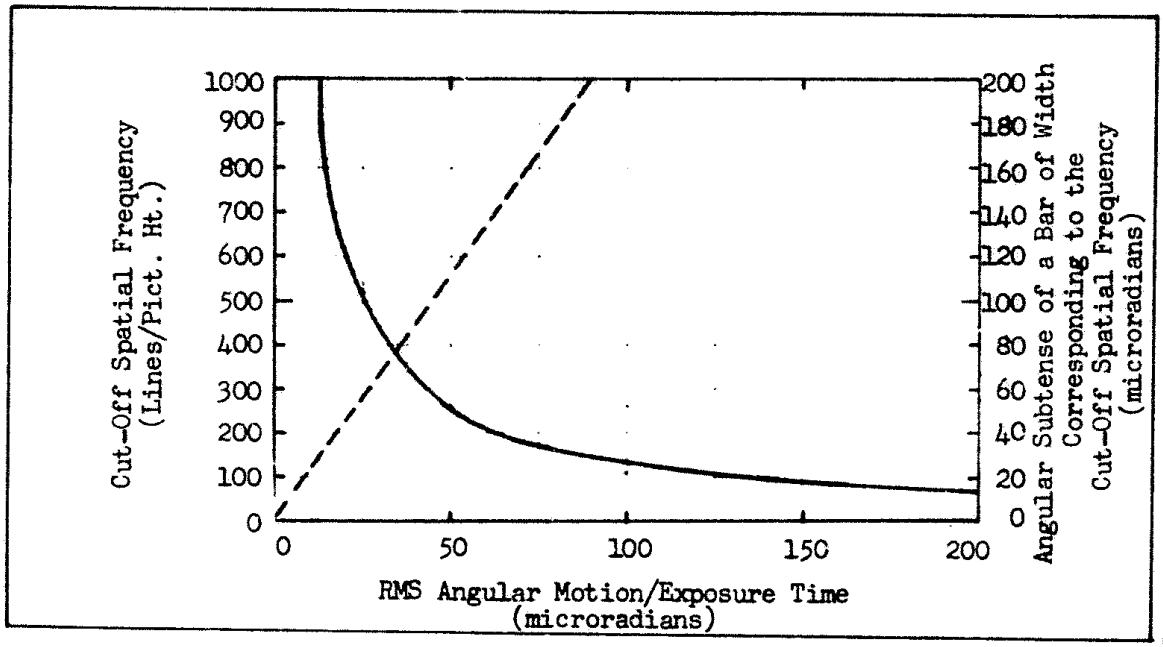

Fig. 35 Cut-off Spatial Frequency and Angular Subtense of Corresponding Period for the Assumed System as a Function of the RMS Angular Motion per Exposure Time. Angular Subtense is Shown as Solid Line.

and is plotted in Fig. 36. Also, the MTF is plotted as a function of the rms image motion amplitude expressed in lines in Fig. 37. Finally, the MTF is shown for the assumed system of Section 2.2 in Fig. 38 together with the effect of a 50 microradian rms motion . As can be seen, the motion MTF completely dominates.

The effect of random motion on system resolution is shown in Fig. 39 in units of lines per picture height and in Fig. 40 in terms of threshold angle. These curves were drawn for an input image modulation of 0.3 and three values of motion (static and 25 and 50 microradians rms). The curves of threshold angle relate most directly to range since range is directly proportional to $\Delta\theta$. With good visibility, reducing the rms motion amplitude by a factor of 2 results in a 50 - 60% range increase.

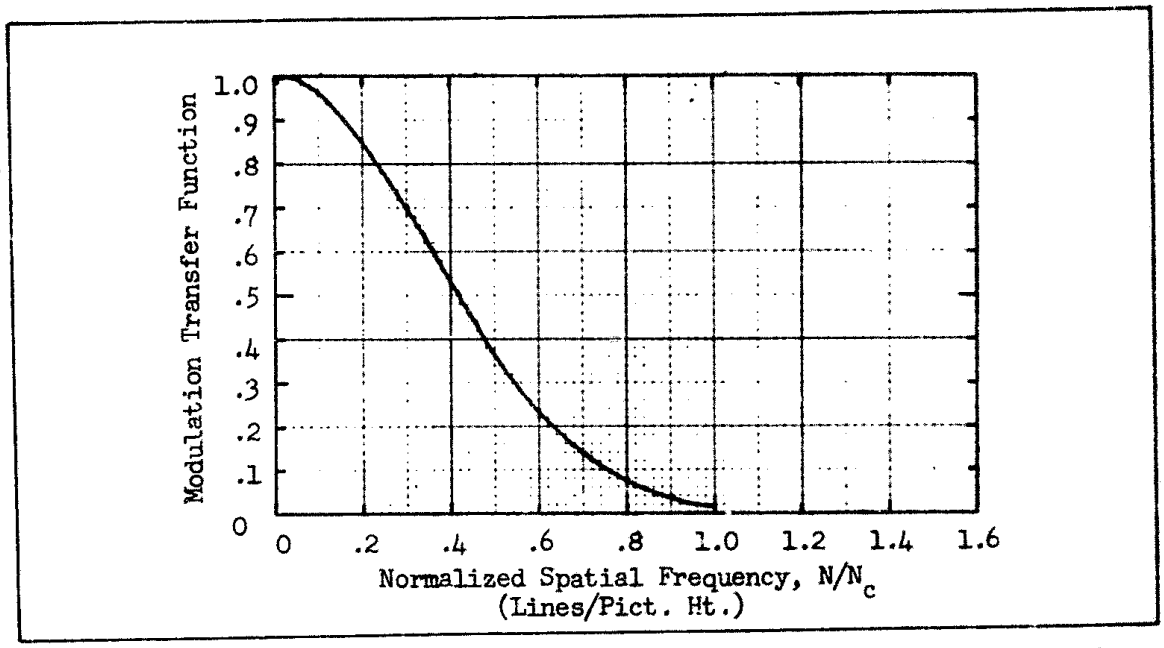

Fig. 36 Modulation Transfer Function vs Spatial Frequency Normalized to the Cut-off Frequency for Random Image Motion.

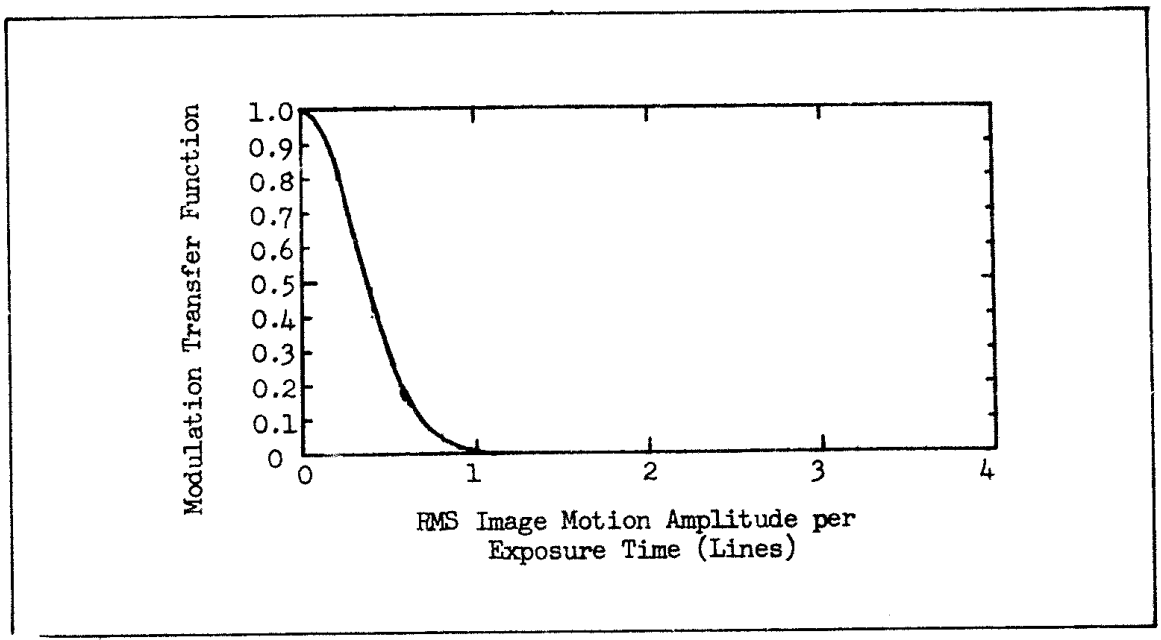

Fig. 37 Modulation Transfer Function for Random Image Motion.

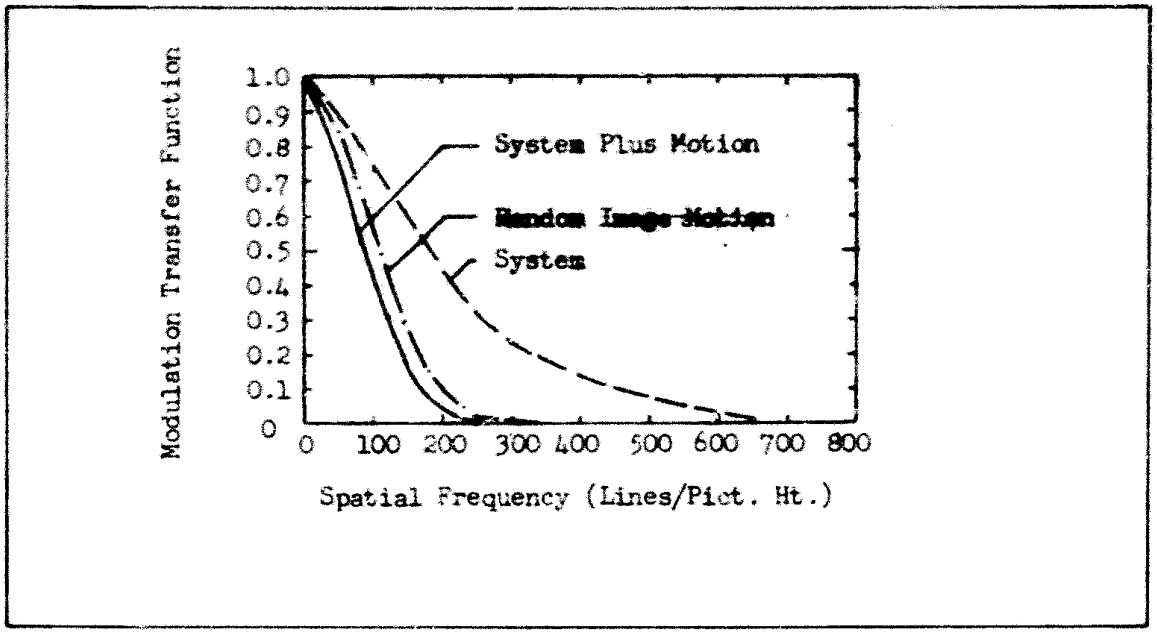

Fig. 38 Modulation Transfer Function for Static System and Scene and for System with Scene in Random Motion of RMS Amplitude 50 microradians with 660 mm Focal Length Lens.

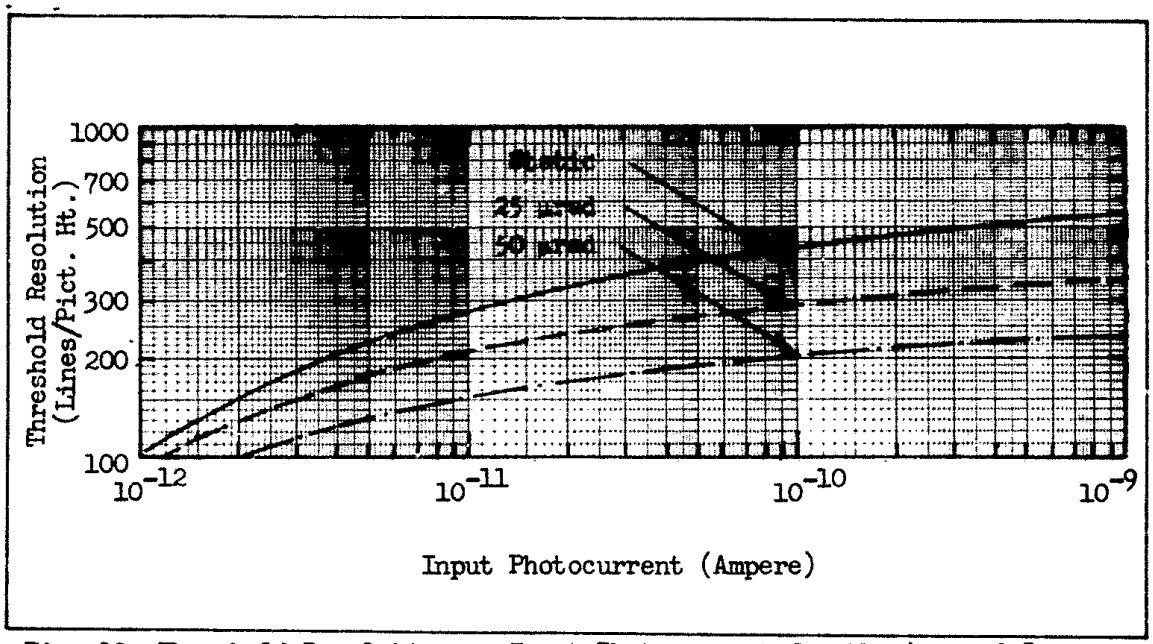

Fig. 39 Threshold Resolution vs Input Photocurrent for the Assumed Sensor with a Static Scene and with Random Motion of the Sightline of Magnitude 25 and 50 μrad. $C_M = 0.3$.

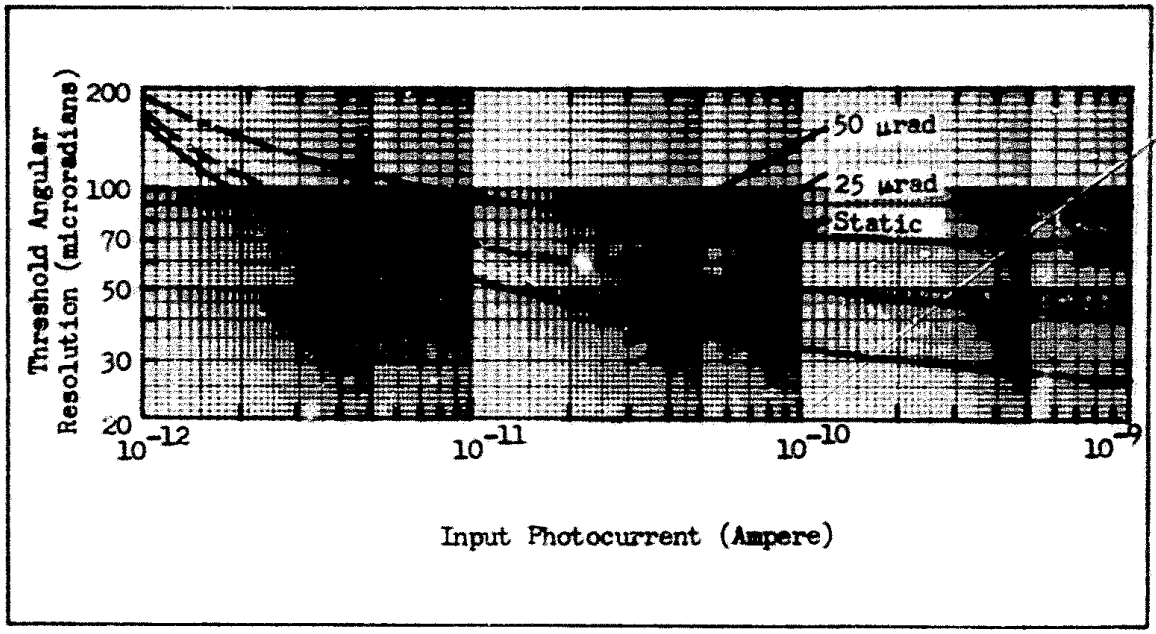

Fig. 40 Threshold Angular Resolution vs Input Photocurrent for the the Assumed Sensor with a Static Scene and with Random Motion of the Sightline of Magnitude 25 and 50 μrad. $C_M = 0.3$.

The angular resolution for the aperiodic and periodic case is shown in Fig. 41. Also shown is the balanced resolution calculated on the basis of the average threshold resolution in lines/pict. ht. These curves were drawn for a random motion of 50 microradian rms amplitude and an input image contrast of 0.1.

In many systems, it is customary to optically zoom the field of view in order to have a wide angle view (WAV) for general navigation and a narrow field of view (NAV) for object recognition. In changing the field of view by say a factor of 4, it is hoped to increase the resolution of scene detail by the same factor. However, in the NAV, the hoped for increase in resolution will not usually be realized because of the more serious effect of motion on the NAV. To show this effect we calculated the limiting resolution for a field of view 4 times larger than

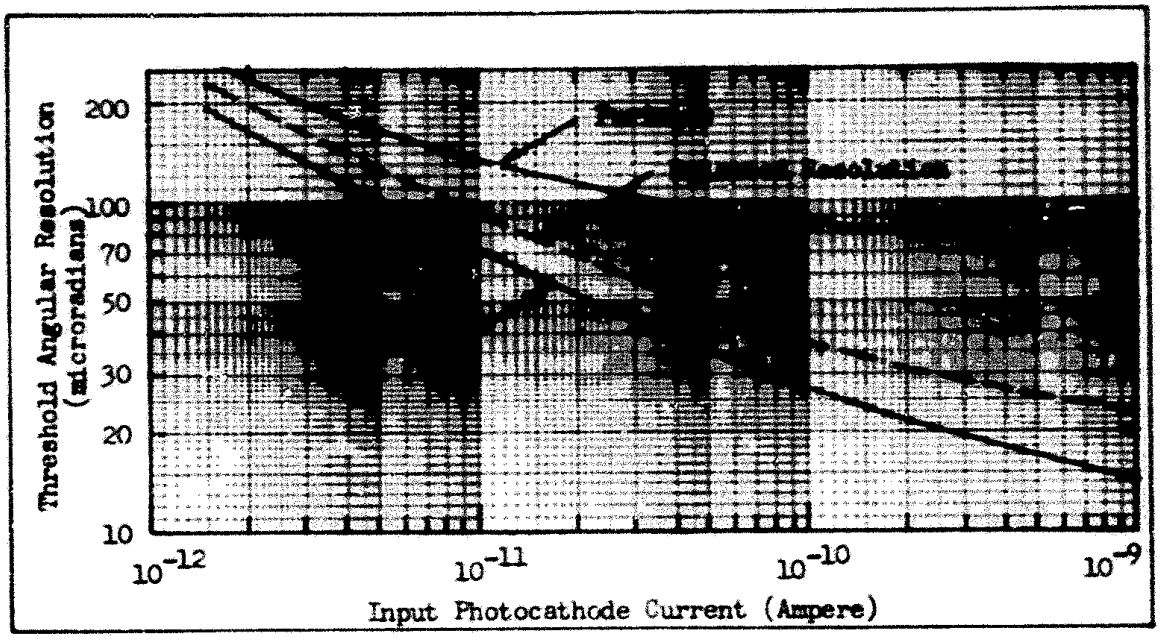

Fig. 41 Threshold Angular Resolution vs Input Photocathode Current Based on the Periodic, Aperiodic and the Average Calculated for the Threshold Resolution in Lines/Pict. Ht. $C_M = 0.1$.

that used in the discussion heretofore with the results shown in Fig. 42. The dashed line, shows the angular resolution in the WAV (about a 4° field of view) and the solid line shows the angular resolution in the NAV (about a 1° field of view). In both cases, the modulation contrast is assumed to be 0.3, the image motion is random of rms amplitude 50 microradians, and the periodic image model was used.

The image appearing on the display is actually 4 times larger in the NAV than in the WAV but the useful magnification, based on threshold angular resolution is much less as can be seen in Fig. 43 where we plot the ratio of angular resolution in the NAV to that in the WAV. At high light levels, the actual effective magnification, when sightline motion is a factor, is only about 2 rather than 4 as ideally expected.

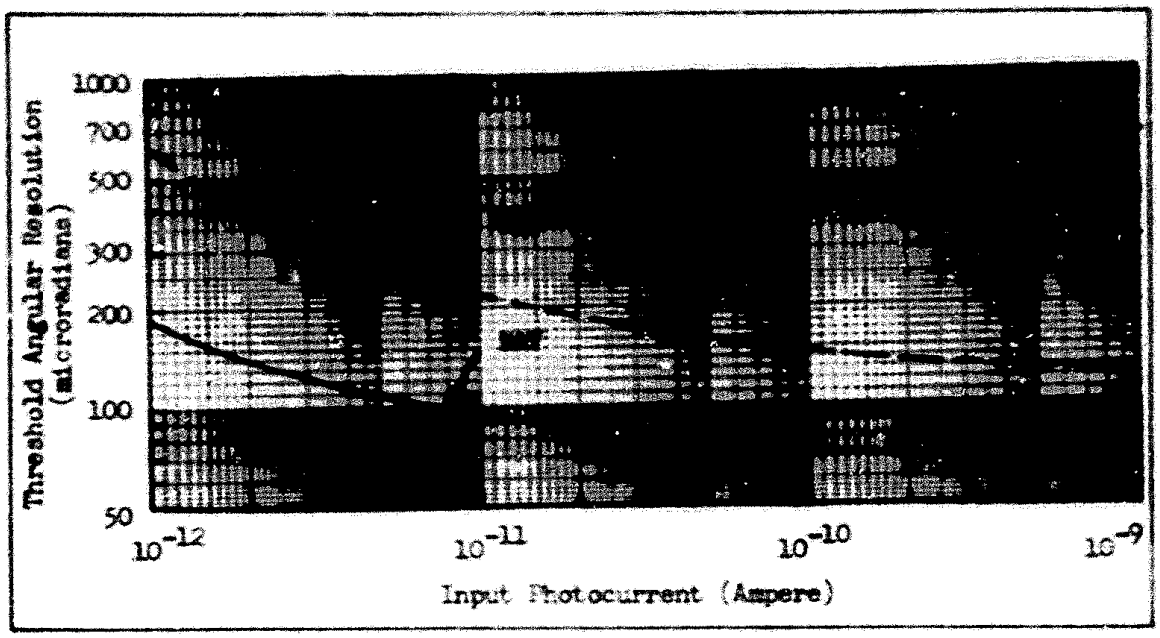

Fig. 42 Threshold Angular Resolution vs Input Photocurrent with a Random Motion of Amplitude 50 microrad RMS for a WAV and NAV. $C_M = 0.1$.

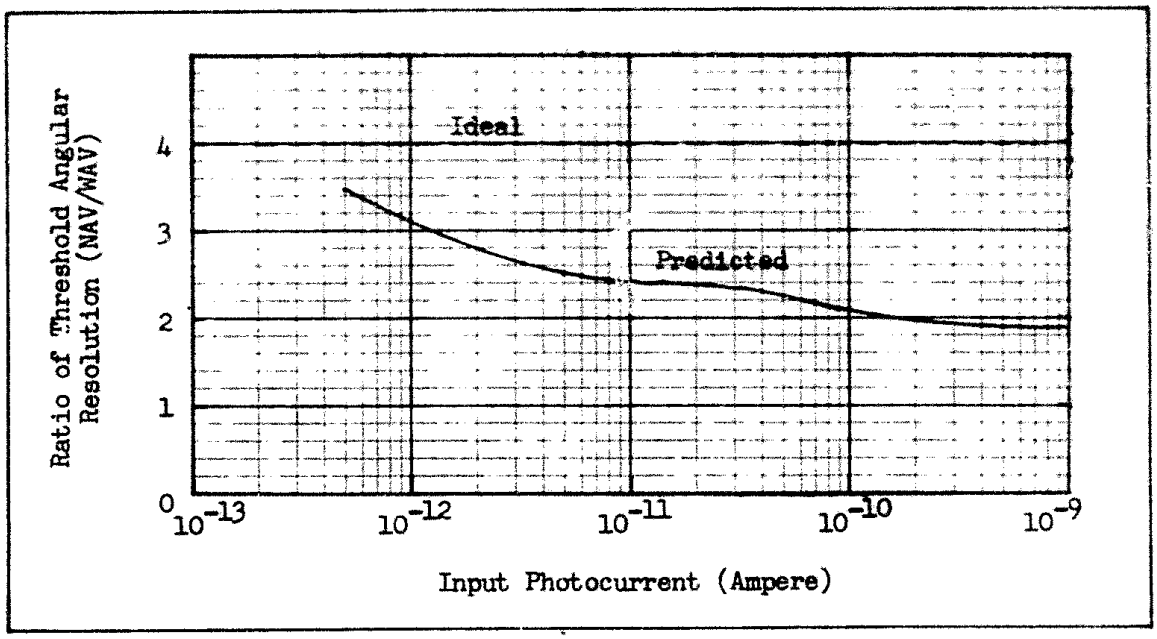

Fig. 43 Ratio of Threshold Angular Resolution in NAV to that in WAV with Random Sightline Motion of Amplitude 50 microrad RMS. $C_M = 0.1$.

The subject of camera time constants will be treated in detail in Section 4 but the results will be briefly reviewed here. The time constants of a camera can be quantitatively thought of as being due to the capacity and resistance of the charge storage surface and the resistance of the reading beam. As an example, consider the EBSICON camera tube which has a photoemissive photocathode and a silicon diode mosaic storage surface. The mosaic is charged by photoelectrons which were accelerated through a large voltage. In the target, the energy of the photoelectrons is converted to hole-electron pairs and the electrons are stored in the capacity of the back biased diodes. With proper design, the RC time constant of the diodes is large enough so that the charge will be retained for a number of frame times which implies that the capacitance of the targets is relatively high (for a given R). For readout, the capacitors are discharged through the resistance of the electron beam and for fastest operation, the capacitance of the target should be small. Clearly a tradeoff is dictated between target storage time and readout time constants. At low signal current operation, the resistance of the electron scanning beam is high and the RC time constant of the readout process is higher than that at high signal currents where the beam resistance is low so a number of frames are required to completely read out the charge. This will have the effect of contrast reduction for dynamic imaging.

Target voltage can also markedly influence the process. A large target voltage, which causes the target capacity to decrease, will decrease the RC time constant, whereas with a low target voltage, the target capacity increases and the RC time constant is larger.

As shown in Section 4, the lag introduced by the RC time constant can be appreciable with low target voltages even though the signal levels are high. Other tubes, with lower prestorage gain such as the I-SEC and I-I-Inocon have even greater lag problems. Dynamic MTF measurements have been made but the results do not appear to fully account for the considerable loss in sensitivity at low spatial frequencies. However, this must be interpreted as an inadequate measurement procedure. Image lag effects will be a major concern in the follow-on program. Because of the preliminary nature of the results obtained so far, we do not propose a method of including lag effects into the analysis at this time. The designer is cautioned, however, that the loss in sensitivity due to lag may be as much as a factor of 4 to 100 at low light levels and due account of lag effects should be made in selecting a sensor for a given application.

2.5 The Balanced Resolution Concept

The effort in sensory system modeling for the purpose of predicting the range at which a real scene object can be discerned is to find a simpler equivalent test object that can be used to replace the real scene object. Presumably, a correspondence can be found between the range at which the real scene object can be discerned with the needed clarity and the range at which the equivalent test object can be detected (or resolved). The simpler equivalent test object should be easy to make and fully amenable to analysis. It is, however, clear that no single test object can be found that will be fully equivalent to all real scene objects which are of infinite variety and complexity. On-the-other-hand, if systems design is to be

anything but a trial and error process, equivalent test objects must be found.

The equivalent bar pattern as suggested by Johnson represents one of the first attempts to find a test pattern which can be used in laboratory evaluation and analysis. This approach makes good sense because it imposes a system resolution requirement. This model was further refined and experimentally tested with the results discussed previously in Ref. 2. The principal deficiency in the concept was in defining the method of measuring the image signals in the real object. It was first thought that the average modulation within the real object could be used but this would require some sort of area weighting. In the end, the maximum signal swing was used which is different than the method of measuring signal swing in the bar pattern which is the mean signal.

A bar pattern, being repetitive, is one of the most difficult of the one-dimensional images to detect and hence it is felt that its use will result in pessimistic predictions. However, in the past, range predicted using the equivalent bar pattern has shown reasonable correlation with range measured for real objects imaged against a terrain background. This is in large part due to the neglect of many important system parameters such as the sky-to-ground brightness ratio, sensor time constants, image motion and display-observer interactions. That is, the pessimistic nature of the equivalent bar pattern prediction obscures other system defects which are, more often than not, neglected. As our knowledge of these system defects

increases, it becomes necessary to take these other factors into account. In particular, when an effect is isolated, such as sightline vibration, it is important that the impact of the effect on range be known. Increases in stability, for example, can be quite costly and the desire will be to evaluate the cost of greater sightline stability vs the improvement in range to be expected.

In an attempt to find a better model, the balanced resolution concept was proposed. The first procedure adopted and rather extensively used in the above is to calculate the resolution based on the equivalent bar pattern and then on a single bar of the bar pattern. For a given set of operating conditions, the calculation results in two values of limiting resolution N_1 and N_2 in lines per picture height. The "balanced" resolution N_b was then taken to be

$$N_b = (N_1 + N_2)/2 \quad . \tag{52}$$

The result of this procedure is shown in angular resolution form in Fig. 41. It is seen that the results are dominated by the aperiodic model and will undoubtedly give far too optimistic results. A possibility is to calculate the aperiodic resolution on the basis of an element of size equal in height and width to the bar width in the equivalent bar pattern.

An alternate approach is to calculate the balanced resolution on the basis of the average angular resolution. This is equivalent to averaging

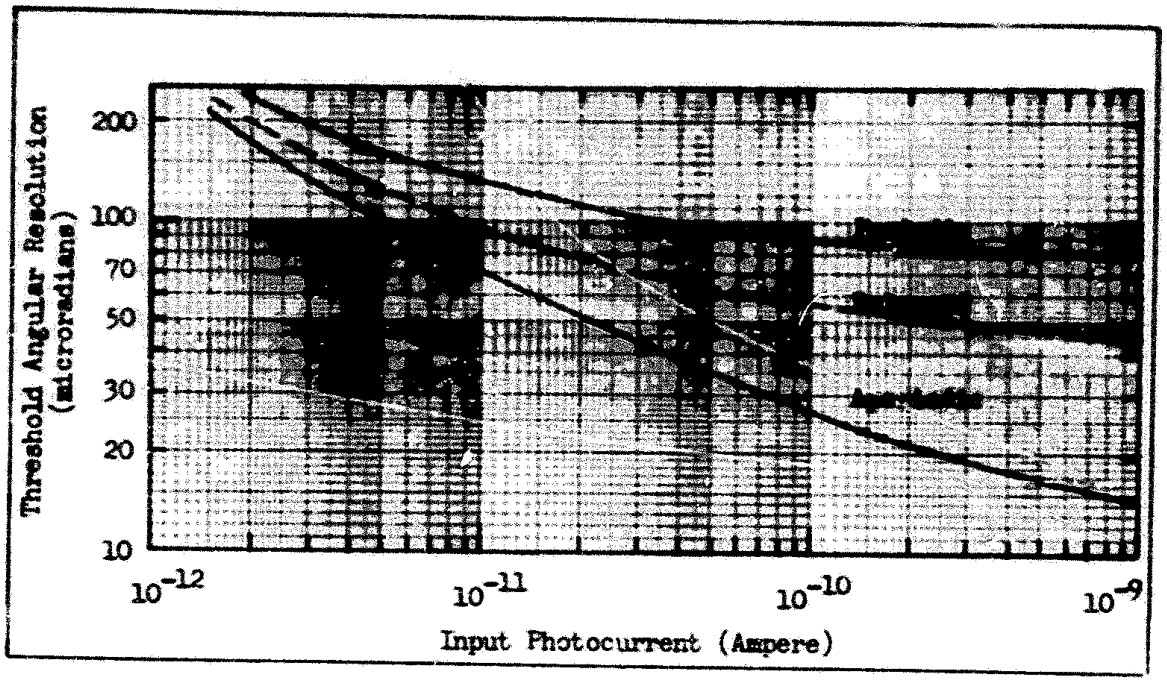

Fig. 44 Threshold Angular Resolution vs Input Photocurrent Based on the Periodic, Aperiodic and the Average Calculated for Threshold Angular Resolution in microradians. $C_M = 0.1$.

$$\Delta\theta_b = (\Delta\theta_1 + \Delta\theta_2)/2$$

$$= \frac{1}{2}\left(\frac{1}{N_1} + \frac{1}{N_2}\right) \quad . \tag{53}$$

This is also equivalent to avereging the ranges calculated using the aperiodic and periodic model. The result of averaging on ar angular basis is shown in Fig. 44. As can be seen, averaging on the angle basis biases the result toward the periodic model.

If a choice were to be made at this point in time, we would tend to favor averaging the results on the angle basis because it gives results better than the pessimistic periodic model but not as optimistic as the aperiodic model which is considered to be excessively optimistic for use in recognition or identification models. The search is, of

course, for a weighting function and, in particular, for one which makes use of the currently well known models that we currently have. However, further efforts are needed to justify the weighting function, whatever it may be, on a retional basis. These first preliminary efforts are for the purpose of examining the impact of certain assumptions.

3.0 Display Signal-to-Noise Ratio Fundamentals

In this section, we will discuss the fundamentals of the display signal-to-noise ratio concept starting with the elementary or ideal model and then adding to the model to bring it into closer correspondence with reality. The elementary model takes into account the image's dimensions, signal levels, and noise levels but otherwise assumes that the image is transmitted through the sensory system with perfect spatial fidelity. The elementary model is then refined by including the effects of finite imaging apertures such as the objective lens, reimaging sensors such as an image intensifier, the TV camera tube and etc. The images and the apertures which alter the image's amplitude, shape and position are analyzed by Fourier methods using the methods of communications theory. An attempt has been made to be general and fairly rigorous in these derivations. We are indebted to Robert L. Sendall of Electro-Optical systems for many of the concepts presented particularly in the area of the aperiodic image treatment.

In Sections 4 and 5, we will discuss some preliminary efforts made to verify the theory. As will be seen, the theory adequately predicts first order effects and many second order effects as well. However, second order effects are quite difficult to measure through psychophysical experimentation partly because of the weak functional dependence of the effects and partly because of the statistical nature of the experimentation.

3.1 The Elementary Model

The historical development of the elementary model was noted and the model was derived in Ref. 2. The purpose of this discussion is to review the elementary model and to give further insight with regard

to its meaning and use. The basic formulation assumes a small rectangular image of area, a, amid a much larger background. Suppose the average number of photoelectrons generated by the sensor's photosurface in time, t, due to the image area, a, is n_2 and the number generated by an equally sized comparison area in the background is n_1. Then the elementary model as derived in Ref. 2 gives the mean signal-to-rms-noise ratio of the image as

$$\begin{aligned} SNR_{pc} &= (n_2 - n_1)/[(n_1 + n_2)/2]^{\frac{1}{2}} \\ &= (\dot{n}_2 - \dot{n}_1)at/[(\dot{n}_1 + \dot{n}_2)at/2]^{\frac{1}{2}} \quad , \end{aligned} \tag{54}$$

where $\dot{n}_1$ and $\dot{n}_2$ are the photoelectron generation rates in units of electrons per unit area and time. The subscript pc is added to SNR to indicate that this is the SNR at the output of the input photosurface. We define the image modulation contrast as

$$\begin{aligned} C_M &= \frac{\dot{n}_2 - \dot{n}_1}{\dot{n}_1 + \dot{n}_2} \\ &= \frac{\dot{n}_2 - \dot{n}_1}{2\dot{n}_{av}} \quad , \end{aligned} \tag{55}$$

so that

$$SNR_{pc} = \frac{2C_M\dot{n}_{av}(at)^{\frac{1}{2}}}{[\dot{n}_{av}]^{\frac{1}{2}}} \quad . \tag{56}$$

In the above derivation, it is assumed that the noise is due to the image photon-to-electron conversion process. When this is the case, the

sensor is said to be photoelectron-noise-limited. For later convenience, the photoelectron rates, $\dot{n}$, are written in terms of the photocurrents, i, as follows

$$i = \dot{n}eA \quad , \tag{57}$$

where e is the charge of an electron and A is the total effective photosurface area. Now, Eq. (56) becomes

$$SNR_{pc} = \left(\frac{at}{A}\right)^{\frac{1}{2}} \frac{2C_M i_{av}}{[ei_{av}]^{\frac{1}{2}}} \quad . \tag{58}$$

In a typical high performance TV camera tube, the image is next transferred to a gain storage target of gain, G_T, and storage time, t_f, so that

$$SNR_T = \left(\frac{at_f}{A}\right)^{\frac{1}{2}} \frac{2G_T C_M i_{av}}{[G_T^2 ei_{av}]^{\frac{1}{2}}} \quad . \tag{59}$$

Note that the signal, $2G_T C_M i_{av}$, and the photoelectron noise, $[G_T^2 ei_{av}]^{\frac{1}{2}}$, are equally amplified with no net result at this point. In TV, the gain storage target is sequentially scanned line-by-line by an electron beam. It is possible to measure a signal-to-noise ratio in the video channel which is given by

$$SNR_{VO} = \frac{2G_T G_V C_M i_{av}}{\sqrt{2(G_T G_V)^2 ei_{av} \Delta f_V}} \quad , \tag{60}$$

where the subscript O in SNR_{VO} refers to the notion that the signal amplitude is not limited by the sensor apertures, G_V is the video amplifier gain, and Δf_V is the video bandwidth. Combining Eqs. (59) and (60), we observe that

$$SNR_D = [2t_f \Delta f_V (\frac{a}{A})]^{\frac{1}{2}} SNR_{VO} \quad . \tag{61}$$

The subscript, D, is added to note that the image signal-to-noise ratio is now referred to the image appearing on a hypothetically perfect display. In the video, the image is frequency upconverted by the electron beam scanning process. In the display, the image frequencies are downconverted by the reverse process, i.e., the electron beam of the cathode ray tube display recreates the original image on the display.

The image area ratio $(\frac{a}{A})$ is dimensionless. This is a convenience in later analysis because the real image area can become larger or smaller as it traverses the system. The use of dimensioned units requires that scale changes be made at each point where the image changes size. But even further, we note that the displayed image can be much larger than the image on the input photosurface. We also note the video gain, G_V, appearing in Eq. (60). By suitably adjusting the d-c level of the display brightness and the video gain, the displayed image can be much brighter and of greater contrast than the image incident on the input photosurface. Thus, in theory, the displayed image can be sufficiently large, sufficiently bright and of high enough contrast

so that the observer's eye, viewing the displayed imagery will be neither acuity, nor contrast, nor displayed-image-brightness limited. If these conditions are met, the SNR_D becomes the SNR_{DI}, the image signal-to-noise ratio generated in the observer's retina provided* that the time, t_f, is changed to the time, t_i, the integration time of the eye.

The above equations represent the image signal-to-noise ratio obtainable from the sensor. The SNR_{DI} required by the observer is determined through psychophysical experimentation as was extensively discussed in Ref. 2. In early work by De Vries (Ref. 7), it was assumed that to be detectable, the image SNR_{DI} must equal or exceed some threshold constant, i.e.,

$$SNR_{DI} \geq K_T = SNR_{DT} \quad . \tag{62}$$

This was verified in Ref. 2 with the typical result shown in Fig. 45 in the form of probability of detection vs signal-to-noise ratio. The threshold signal-to-noise ratio, SNR_{DT}, corresponding to a 50% probability of detection, is very nearly a constant, independent of image size for most of the image sizes of interest (the exceptions are noted in Ref. 2).

As previously noted in Section 2.1, it is hypothesized that an observer must detect the presence of a single bar in a bar pattern to discern the presence of a bar pattern. Thus, Eqs. (59) and (61) apply.

---

* Assuming continuous presentation of the scene on the display.

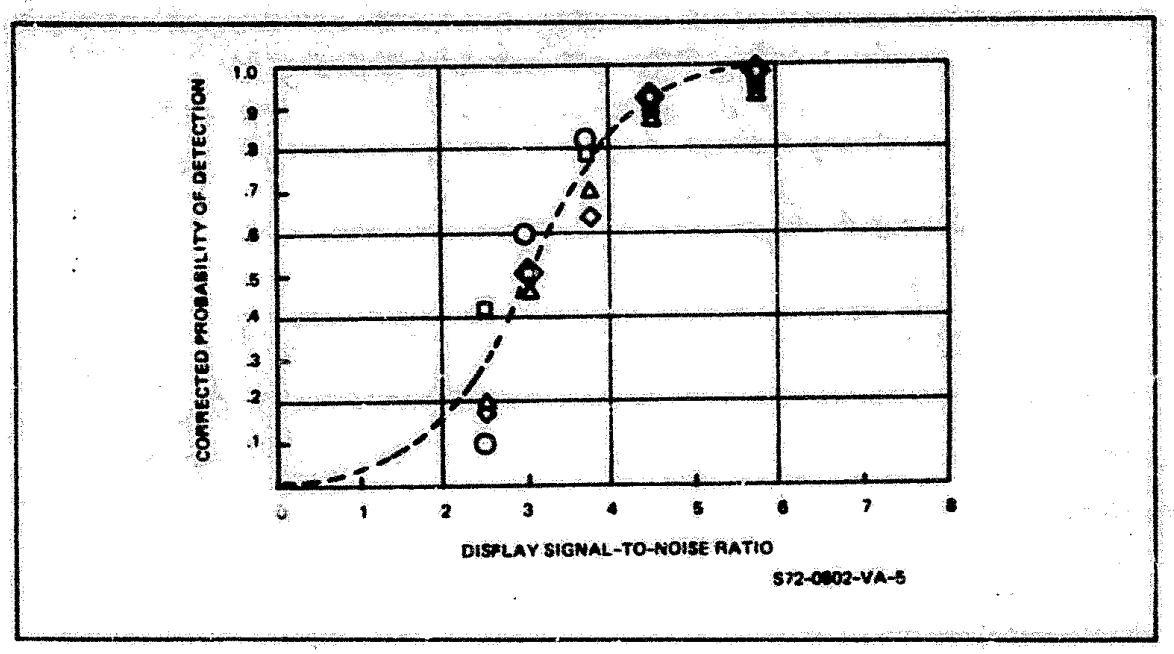

Fig. 45 Corrected Probability of Detection vs SNR_{DI} Required for Rectangular Images of Size ○4 x 4, □4 x 64, Δ 4 x 128 and ◇4 x 180 lines.

However, it is usual to rewrite Eq. (61) in the form

$$SNR_{DI} = \left[\frac{2t_i e \Delta f_V}{\alpha}\right]^{\frac{1}{2}} \frac{1}{N} \; SNR_{VO} \quad , \tag{63}$$

by use of Eqs. (2) and (3) and the area relation, $A = \alpha Y^2$.

Again, through psychophysical experimentation, the threshold signal-to-noise ratios were determined with the typical result shown in Fig. 46. As for aperiodic images, we note that the SNR_{DT} is approximately a constant over a wide range of spatial frequencies. The equations above apply to the case where the primary noise is that generated in the primary photoconversion process. If a system noise, such as preamp noise of rms value, I_p, in bandwidth Δf_V is added subsequent to the sensor gain, then

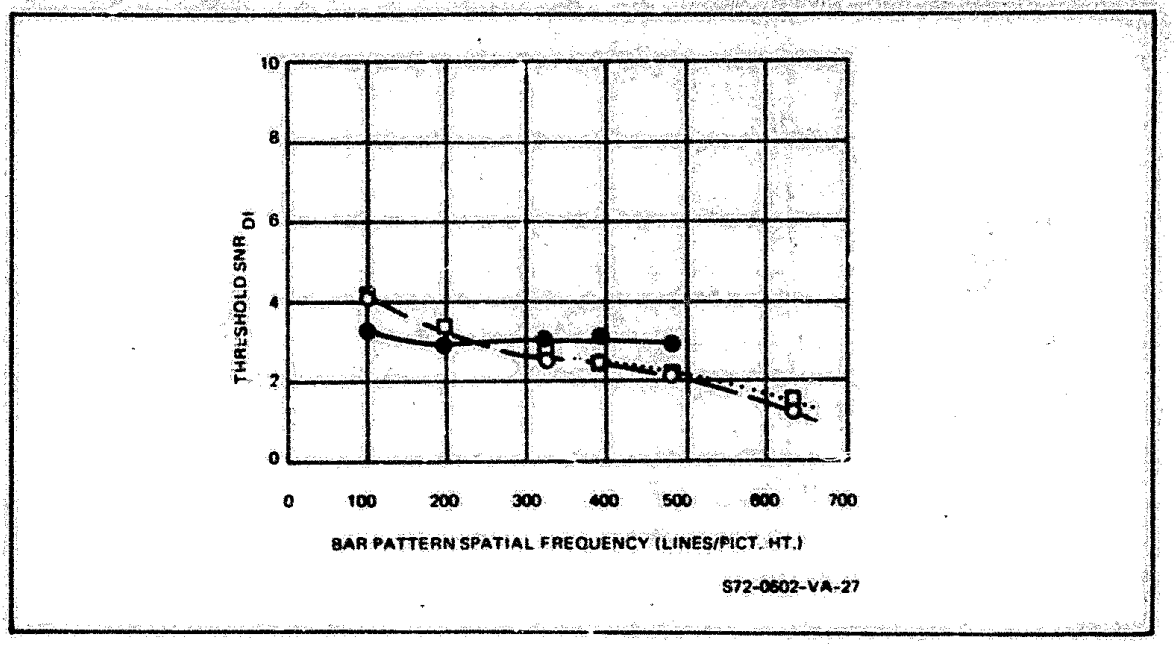

Fig. 46 Threshold SNR_{DI} vs Bar Pattern Spatial Frequency for Display-to-Observer Viewing Distances of ○ 14", □ 28" and ● 56".

$$SNR_{DI} = \left[\frac{\rho t_i}{A}\right]^{\frac{1}{2}} \frac{2G_T C_M i_{av}}{\left[G_T^2 ei_{av} + I_p^2/2\Delta f_V\right]^{\frac{1}{2}}} \quad , \tag{64}$$

for the aperiodic model and,

$$SNR_{DI} = \left[\frac{t_i \epsilon}{\alpha}\right]^{\frac{1}{2}} \frac{1}{N} \frac{2G_T C_M i_{av}}{\left[G_T^2 ei_{av} + I_p^2/2\Delta f_V\right]^{\frac{1}{2}}} \quad , \tag{65}$$

for the periodic model. In both cases, the added system noise is assumed to be white.

Before continuing, we note that many analysts and experimenters choose to define the threshold signal-to-noise ratio in terms of the video singal-to-noise ratio, SNR_{VOT}. For the periodic image case, this results in the equation

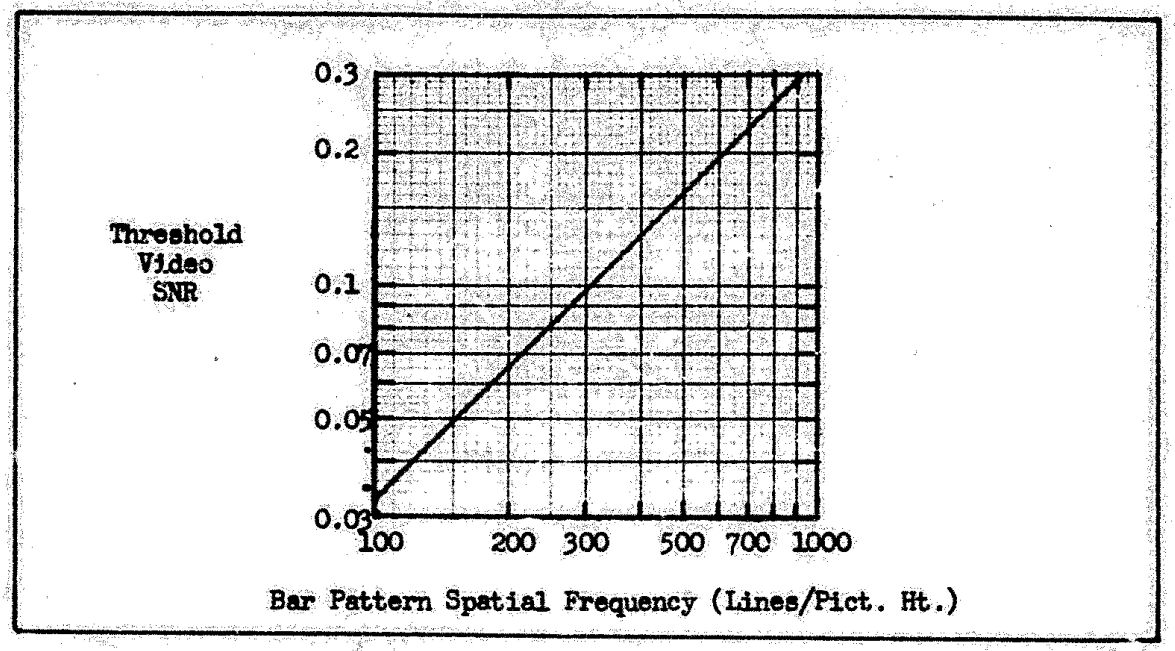

Fig. 47 Threshold Video SNR vs Bar Pattern Spatial Frequency for a Video Bandwidth of 10^7 Hz.

$$SNR_{VO-T} = \frac{N \bullet SNR_{DT}}{\left[\frac{2t_i \epsilon \Delta f_V}{\alpha}\right]^{\frac{1}{2}}} \qquad (66)$$

For $t_i = 0.1$ sec, $\epsilon = 5$, $\Delta f_V = 10^7$ Hz and $\alpha = 4/3$, $SNR_{VO-T} = 1.16 \times 10^{-4}$ SNR_{DT} and for $SNR_{DT} = 2.8$, we plot the SNR_{VO-T} in Fig. 47. This curve or some variation of it is sometimes called the "eye modulation demand function." The inference is that as image's spatial frequency increases, the eye "demands" more signal modulation. The use of this curve is generally to be deplored. First of all, if the spatial frequency of the pattern is too high, the observer should be able to move closer to the display and thereby reduce the threshold. But the threshold does not decrease. Furthermore, instead of a single number for a threshold, a curve

becomes necessary. Finally, system parameters become mixed with observer parameters which is an inconvenience when observer-display interactions are to be considered.

With this short review of the elementary model, we proceed to the treatment of finite apertures.

3.2 The Effect of Finite Apertures on Image Detail

If an imaging device were perfect, a point source would appear as a point in the image's plane. If this were so, all images would be transmitted through the device with perfect fidelity. In reality, images will differ from the object in amplitude, shape or phase (position) or all three. These image changes are due to finite imaging apertures such as those associated with a lens, a fiber optic faceplate, an electron scanning beam, a phosphor particle and the like. In the case of a lens, the limiting aperture may be the lens diameter or an iris placed before it. In a fiber-optic faceplate, it is the diameter of the fiber itself. Whatever their form or cause, their effect is to smear image detail in a manner analogous to the filtering of electrical signals by electrical filter networks.

To illustrate the effect of an aperture, consider the point source object of Fig. 48(a). Due to diffraction, chromatic and geometric aberrations, and imperfect focusing, the point will be imaged by the lens as a blur. A line source as shown in Fig. 48 (b) will be similarly blurred. An equation representing the image intensity vs the x, y coordinates in the image plane is known as the point spread function or impulse response. For the line, the one-dimensional equation is known as the line spread function. The line spread case corresponds most directly to the

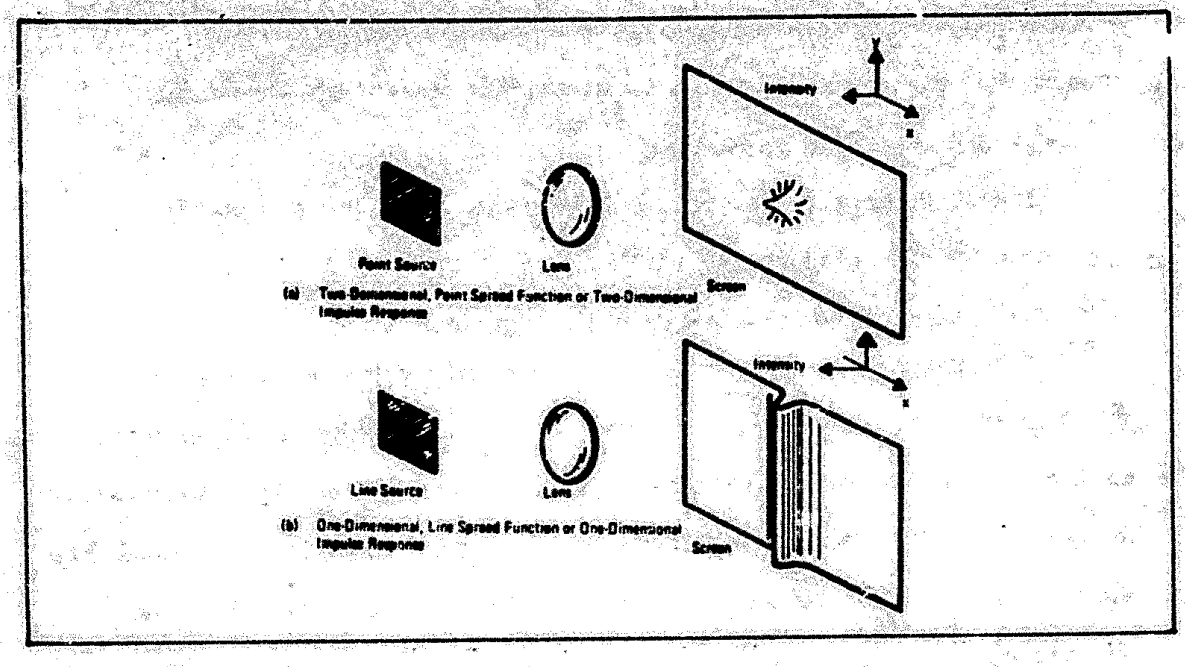

Fig. 4.8 Effect of an Aperture on a Point and Line Source Image.

radio communications case where the signals vary only in amplitude and time. However, the two-dimensional aspects of a point image do not impose unusual conceptual difficulties.

A linear aperture is one which has a response to several input signals acting simultaneously, that is identical to the sum of the responses that each signal would produce individually. This property of linearity leads to considerable simplification in the mathematical description of such phenomena. In particular, it becomes possible to decompose complicated input signals to simpler signals for which the system response is known and then find the total response by summing the individual responses in linear combination. Furthermore, we can then use Fourier analysis in which the complicated input signals are decomposed to sine and cosine waves.

The Fourier transform of a complex function $f(x,y)$ of two independent

variables, x and y, is given symbolically by $F(k_x,k_y)$ and is defined by

$$F(k_x,k_y) = \iint_{-\infty}^{\infty} f(x,y)\exp[-j2\pi(k_x x + k_y y)]dxdy \quad . \tag{67}$$

The complex quantities, k_x and k_y, are referred to as spatial frequencies and are also independent. The original function, $f(x,y)$, can be recovered by taking the inverse Fourier transform as follows

$$f(x,y) = \iint_{-\infty}^{\infty} F(k_x k_y)\exp[j2\pi(k_x x + k_y y)]dk_x dk_y \quad . \tag{68}$$

Some further properties of the Fourier transform are discussed in Reference 8 but a general familiarity with Fourier techniques is assumed.

One of the most important imaging system test objects is the point source. In more glamorous terminology, the point source is known as the Dirac delta function, the unit volume impulse or, the zero order singularity test function. Symbolically, it is designated $\delta_o(x - x_1, y - y_1)$ and has the property of being of infinite amplitude at $xy = x_1, y_1$ and zero everywhere else. Also,

$$\iint_{-\infty}^{\infty} \delta_o(x - x_1, y - y_1)dxdy = 1.0 \quad , \tag{69}$$

and, the Fourier transform of $\delta_o(x - x_1, y - y_1)$, is

$$F(k_x,k_y) = 1.0 \quad . \tag{70}$$

That is, the frequency response of the Dirac delta function is unity everywhere in frequency space. Thus, the Dirac delta function can be thought of as a point image of infinite amplitude but finite volume in

x,y space and of uniform distribution in spatial frequency space over all frequencies. This frequency distribution is often known as a white spectrum.

The response of any finite aperture, be it a lens, photosurface, electron beam, or whatever, to the Dirac delta function is designated $r_o(x,y)$ in the space domain and $R_o(k_x,k_y)$ in the Fourier spectrum. The quantity $r_o(x,y)$ is the point spread function or impulse response and $R_o(k_x k_y)$ is known as the optical transfer function, or OTF, or alternatively as the complex-steady-state-frequency response. If either $r_o(x,y)$ or $R_o(k_x,k_y)$ are known, then the aperture's response to any input test signal can be determined, i.e., these functions completely specify the parameters of the aperture. In general, the OTF may be written in the form

$$R_o(k_x k_y) = \left|R_o(k_x k_y)\right| \exp[j\varphi(k_x,k_y)] \ . \tag{71}$$

The quantity $\left|R_o(k_x k_y)\right|$ has been designated the modulation transfer function, or MTF, and $\varphi(k_x,k_y)$, the phase transfer function, or PTF.

Whenever image intensity distributions are analyzed by Fourier means, it is the practice to normalize the frequency distribution in the following manner. Suppose the intensity distribution is $g_i(x,y)$, then the normalized spectrum is

$$G(k_x,k_y) = \frac{G_i(k_x,k_y)}{G_i(o,o)} \tag{72}$$

where

$$G_i(o,o) = \iint_{-\infty}^{\infty} g_i(x,y)\,dx\,dy \tag{73}$$

as can be seen from Eq. (67). The normalization of the spectra by their

"zero frequency" values is partly for convenience but has a fundamental reason. Since intensity is a non-negative quantity, an intensity distribution always has a non-zero "dc-component" or constant background. The visual quality of an image is, to a large extent, dependent on the contrast or relative intensities of the information bearing portions of the image above or below the ever present background and hence, the spectra are normalized by that background (Ref. 8). The OTF is also normalized and has a value of unity at zero frequency. Also, the conjugate of the OTF, $R_o^*(k_x,k_y) = R_o(-k_x,-k_y)$ and, the value of the OTF at frequencies above zero is always less than unity. These conditions are, of course, properties of linear apertures and do not apply to non-linear elements.

It is further noted that while the OTF is always unity at zero frequency, it is not implied that the absolute intensity level of the object is the same as the absolute intensity of the object's image. In the case of a lens, the absolute image intensity level is always less than that of the scene due to the lens' finite entrance aperture; a decrease which is not evident in the OTF because of the way OTF is normalized.

In the general discussion, spatial frequency has been expressed in line pairs per unit distance. Usually, either k_x or k_y are given in line pairs/mm. This is sometimes a convenience in specifying the OTF of a lens which can be used with a number of film formats and because film OTF's are often given in the same units. In more complex systems, where a number of imaging and re-imaging steps may be involved, the line pair/mm units are not so handy. For example, in a low-light-level television

camera, the input image, the image at the output of the intensifier, the image at the gain-storage target and the displayed image may all be a different size. One of the principal merits of describing various aperture responses in the frequency domain is that the overall response of a number of apertures in cascade can be determined by simple multiplication of the individual responses. However, when image magnifications and minifications are involved as in the LLLTV, direct multiplication is not possible — a scale change must be made at each OTF interface.

The scale change complexity, due to changes in picture size, can be avoided by expressing resolution in terms of the picture height. This is true in TV practice where the specific units used are lines or half cycles per picture height. In the following, we will use the TV nomenclature except when otherwise specified. To avoid confusion, we will give the symbol N to resolution expressed in these terms. For this case, the Fourier transform pair equations become

$$F(N_x,N_y) = \int_{-\infty}^{\infty}\int f(x,y) \cdot \exp[-2\pi(N_x x + N_y y)] \cdot dx \cdot dy \qquad (74)$$

$$f(x,y) = \frac{1}{4}\int_{-\infty}^{\infty}\int F(N_x \cdot N_y) \exp[j\pi(N_x x + N_y y)] \cdot dN_x dN_y \ , \qquad (75)$$

when results are plotted in terms of N, lines per picture height, they can be converted to line pairs per millimeter at any point using the formula

$$k_x = N_x/2Y \ , \qquad (76)$$

where Y is the picture height in mm.

Another unit of interest is the angular measure, k_θ, which is spatial frequency expressed in line pairs per milliradian which is related to N by

$$k_{\theta x} = \frac{N_x \cdot F_L}{2000Y} \quad , \tag{77}$$

where F_L is the lens focal length.

To clarify these measures, suppose that a repetitive bar pattern is projected onto an image plane. Let the bar pattern spacing be Δy in mm. The spatial frequency k is the number of cycles, equal to $2\Delta y$ in length which can be fitted into 1 mm. Thus,

$$k = \frac{1}{2\Delta y} \quad . \tag{78}$$

If the picture height is Y mm, N is the number of half cycles equal to Δy in length that can be fitted into Y, i.e.,

$$N = Y/\Delta y \quad . \tag{79}$$

The angular subtense, $\Delta\theta$, of Δy in mr, with a lens of focal length, F_L, is $1000\Delta y/F_L$. The spatial frequency k_θ is the number of cycles of length $2\Delta\theta$ which can be fitted into a milliradian. Thus,

$$k_\theta = \frac{1}{2\Delta\theta} = \frac{F_L}{2000\Delta y} \quad . \tag{80}$$

In general, k_θ will be used only to describe overall sensory system resolution.

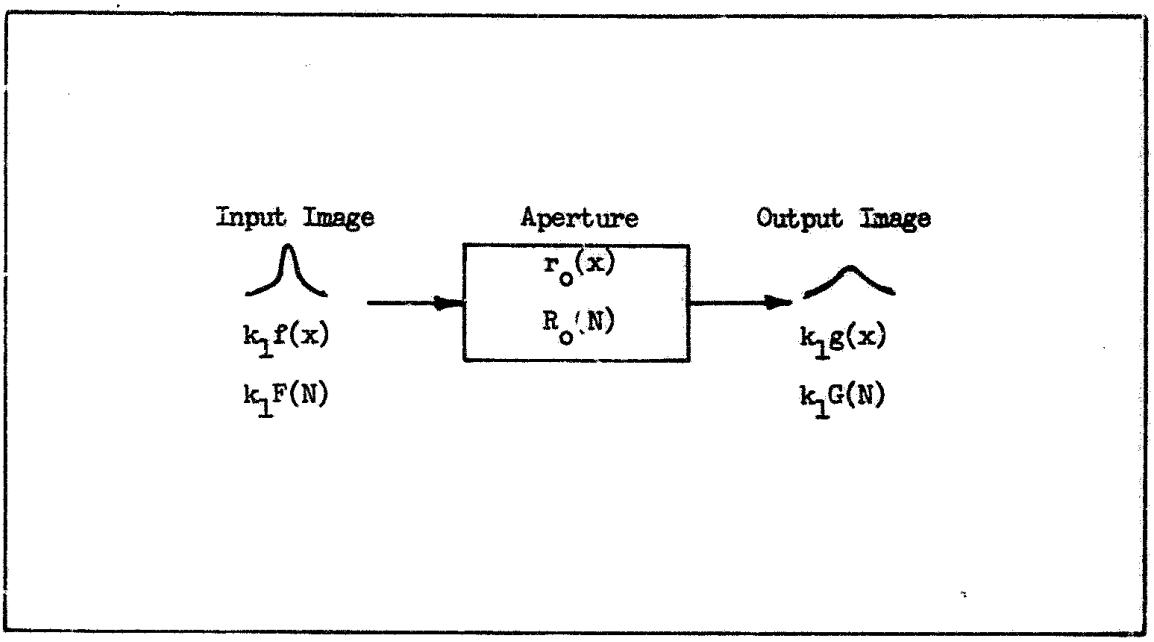

Fig. 49 Schematic of the Input-Output Relationships for an Aperture.

An aperiodic object, as used here, is an isolated object viewed against a uniform background of large extent. For practical purposes, a background can be considered to be of large extent when the object is sufficiently far removed from other objects so that the image of the object, after being smeared out by the apertures through which it passes, does not become additively combined with the smeared out images of other objects in the viewed scene.

The general nomenclature we shall use for analysis of one-dimensional objects is shown in the functional diagram of Fig. 49. In the space domain, the input signal is $k_1 f(x)$, the aperture is $r_o(x)$ and the output is $k_1 g(x)$ where $g(x)$ is the convolution of $r_o(x)$ and $f(x)$, i.e.,

$$g(x) = r_o(x) * f(x) \quad . \quad . \tag{81}$$

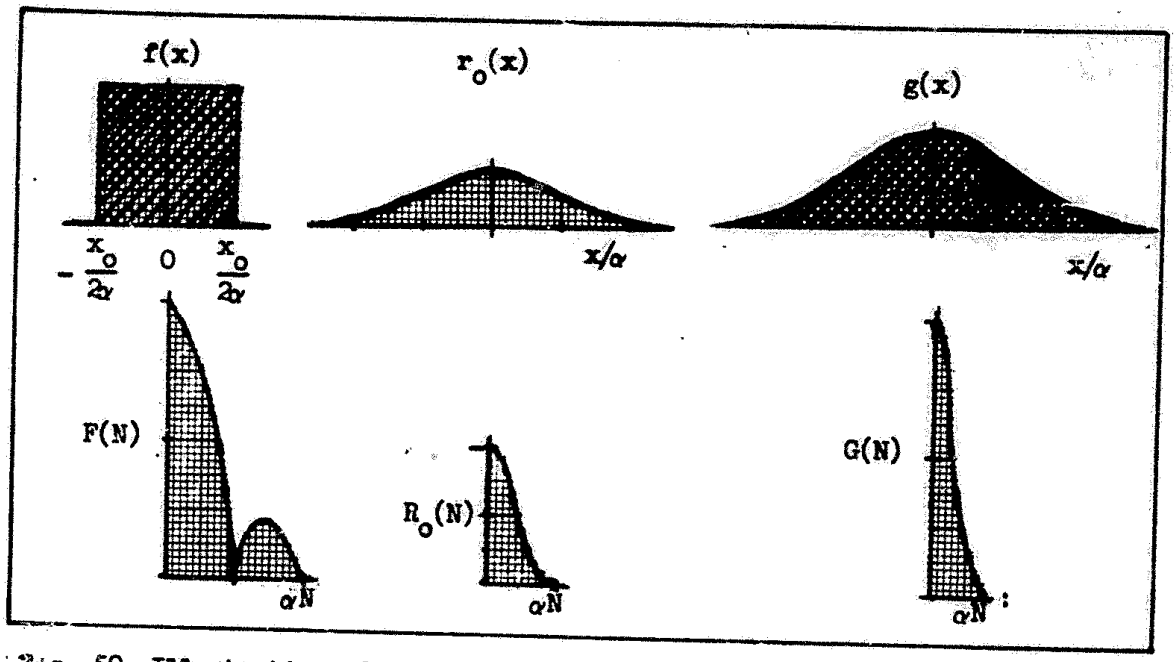

Fig. 50 Illustration of the Effect of an Aperture of Effective Duration $x_o/\alpha = 1.0$ on a Rectangular Input Image in Both the Space and Fourier Domains for $x_o/\alpha = 2.0$.

Similarly in the spatial frequency domain

$$G(N) = R_o(N) \bullet F(N) , \tag{82}$$

where $G(N)$, $R_o(N)$ and $F(N)$ are the Fourier transforms of $g(x)$, $r_o(x)$ and $f(x)$. These processes are illustrated graphically in Fig. 50 for the special case of a rectangular input signal and a Guassian aperture of the mathematical form

$$r_o(x) = \left[\exp[-\tfrac{1}{2}(\tfrac{x}{\alpha})^2]\right]/(2\pi\alpha^2)^{\frac{1}{2}} , \tag{83}$$

and

$$R_o(N) = \exp[-(\pi\alpha N)^2/2] . \tag{84}$$

A unit amplitude rectangular input image can be described by either

$$f(x) = \begin{cases} 0 & x < -\frac{x_o}{2\alpha} \\ 1 & -\frac{x_o}{2\alpha} \le x \le \frac{x_o}{2} \\ 0 & x > \frac{x_o}{2\alpha} \end{cases} \tag{85}$$

or

$$F(N) = \frac{x_o}{\alpha} \frac{\sin(\pi\alpha N x_o/2\alpha)}{(\pi\alpha N x_o/2\alpha)} \quad . \tag{86}$$

The effect of passing the above rectangular image through the Guassian aperture of Eqs. (83 and 84) above is illustrated in Fig. 50 for the case of $x_o/\alpha = 2$. For this case, the input signal is near the same size as the aperture, so the aperture has a pronounced effect on it.

The Fourier spectra of pulses of width $x_o/\alpha = 8$ and 4 are shown along with $R_o(N)$ for the assumed Guassian aperture in Fig. 51. It is seen that the MTF should have little effect on the pulse of width 8 but a more pronounced effect on the pulse of width 4. This is in fact the case as can be seen in Fig. 52 where the output wave shapes for various pulses of width x_o/α= 16, 8, 4 and 1 are shown. The outputs pulses are plotted as dashed curves while the input pulses are plotted as solid curves. It is seen that as the input pulses become progressively smaller, the first effect is to round the output pulse corners leaving peak amplitude unchanged. As the input pulse approaches the effective width of the point spread function, $r_o(x/\alpha)$, the amplitude decreases as well. The change in pulse amplitude is shown as a function of the input pulse width in Fig. 53. When the input pulse is wide, the effective

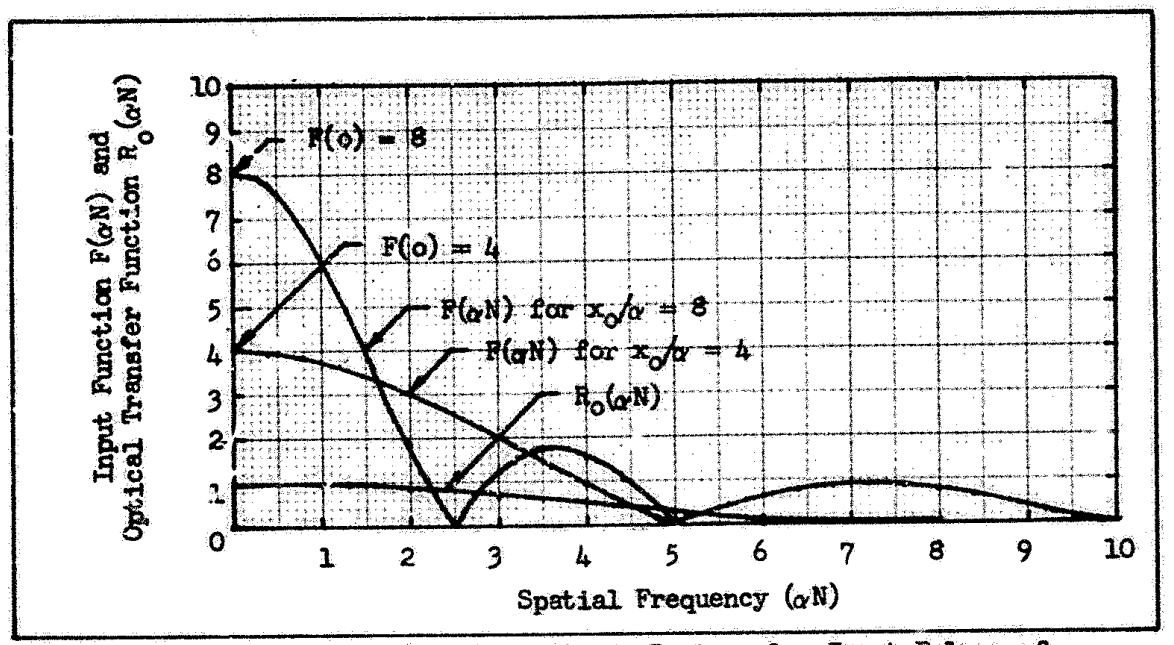

Fig. 51 Fourier Spectra of Unit Amplitude Rectangular Input Pulses of Duration $x_o/\alpha = 8$ and 4. Also shown is the Optical Transfer Function for a Guassian Impulse Response of Effective Duration $x_o/\alpha = 1$.

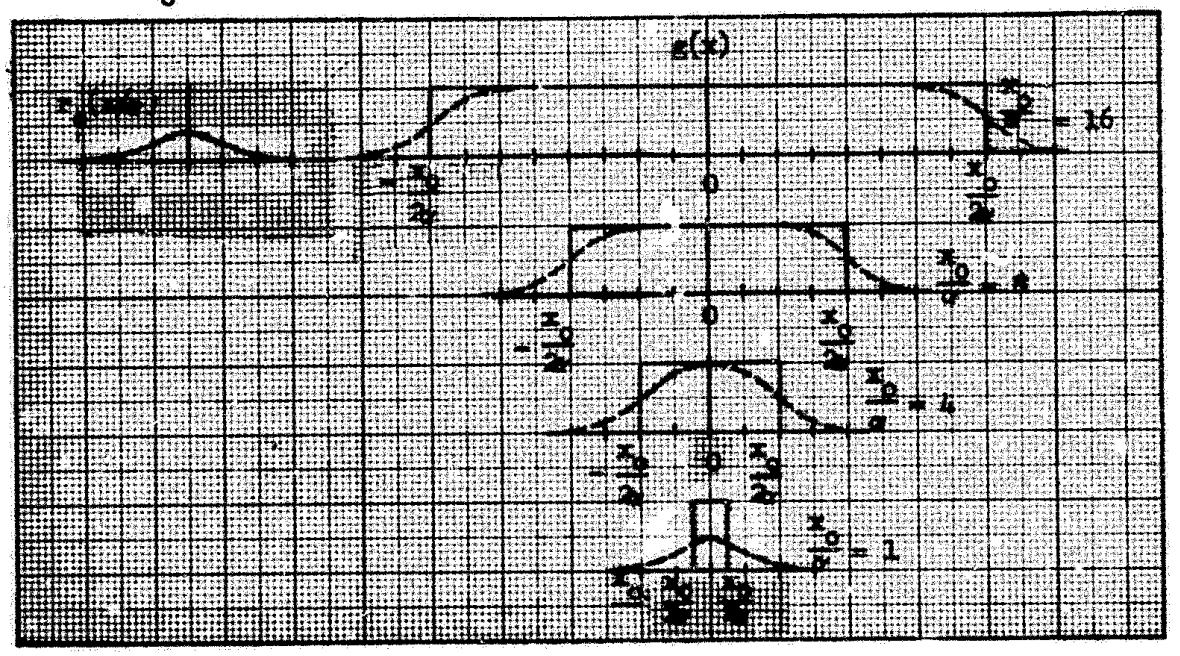

Fig. 52 The Effect of a Guassian Impulse Response on (——) Unit Amplitude Rectangular Input Pulses of Duration 16, 8, 4, and 1. Output Waveshape is Shown as Dashed Curve.

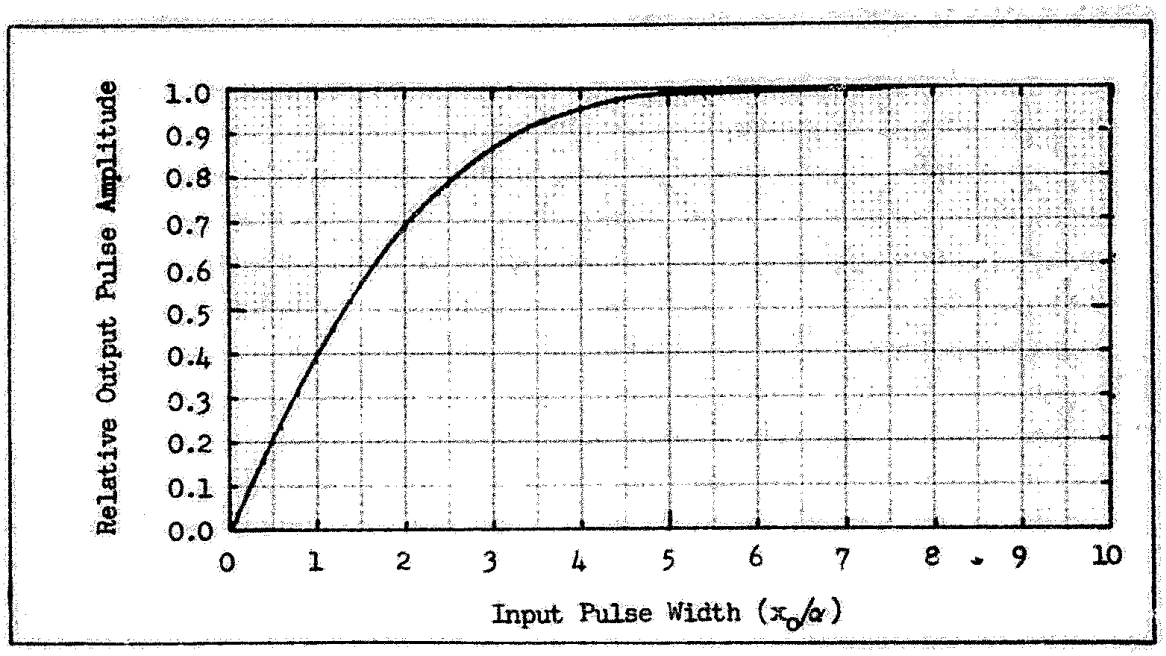

Fig. 53 Relative Output Pulse Amplitude vs the Width of a Unit Amplitude Rectangular Pulse after Filtering by a Guassian Aperture of Effective Duration, $x_o/\alpha = 1.0$.

width of the output pulse is almost equal to that of the input pulse. As the input pulse becomes very narrow, the effective width of the output pulse becomes very nearly a constant independent of the width of the input pulse as can be seen from the curve of Fig. 54.*

In the elementary theory of imaging, it is assumed that the eye, within certain bounds, can expand its limits of integration as necessary to match the dimensions of a displayed image and that the perceived signal, s_p, will be proportional to the area of the displayed image.

---

* In plotting the effective width, it was assumed that the width is equal to the width of a rectangle of height equal to the output pulse amplitude and area equal to the output (or input) pulse. This is not the noise integration distance to be discussed later.

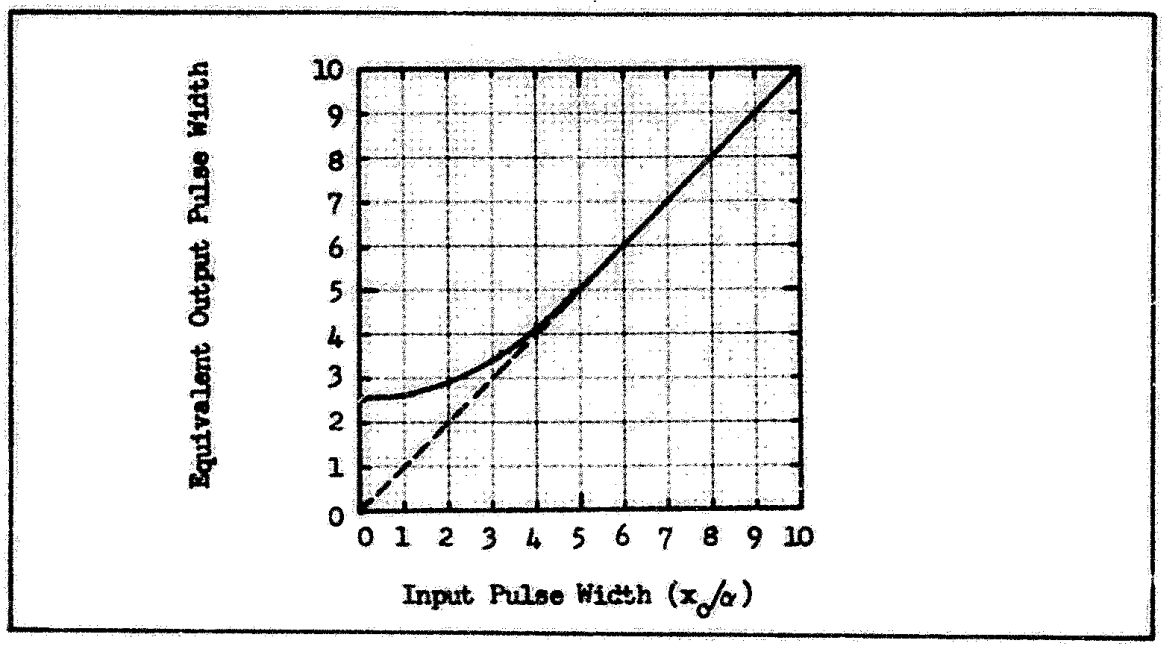

Fig. 54 Equivalent Output Pulse Width vs the Width of a Unit Amplitude Rectangular Input Pulse of Width x_o/α After Passing Through a Guassian Aperture of Equivalent Width $x_o/\alpha = 1.0$.

Specifically,

$$s_p = k_1 t \int_{-\infty}^{\infty} g(x)dx \quad , \tag{87}$$

where k_1 is the incremental amplitude of the input pulse, and t is the integration time of the observer's eye. Observe that

$$G(N) = \int_{-\infty}^{\infty} g(x)\exp(-j\pi Nx)dx \quad , \tag{88}$$

and that

$$G(o) = \int_{-\infty}^{\infty} g(x)dx \quad . \tag{89}$$

That is, the integral over the output area image is equal to the value of

the Fourier transform of the output image at zero frequency.

We further note that from Eq. (79),

$$G(o) = R_o(o) \cdot F(o) \tag{90}$$

and since $R_o(o)$, the value of the OTF at zero frequency is equal unity by definition, $G(o) = F(o)$ and

$$\begin{aligned} s_p &= k_1 t\ G(o) \\ &= k_1 t\ F(o) \\ &= k_1 t \int_{-\infty}^{\infty} f(x)dx \quad . \end{aligned} \tag{91}$$

The implication of the above result is that the area under the output pulse in Fig. 50 is identical to the area under the input pulse as is also shown by the hatched areas in the figure. Thus, if our assumption concerning the spatial integrating capability of the eye is correct, the aperture has no effect on the perceived signal, i.e., as the image is spread out by the aperture, the eye merely expands its limits of integration to include all of the signal.

While the aperture does not affect the perceived signals, it can affect the perception of noise added either prior to or subsequent to an aperture. To begin, assume that noise is added after the image has passed through the aperture as shown in Fig. 55. Suppose the input pulse is rectangular as shown by the dashed lines and that the output pulse is smeared out as shown by the solid curve. In general, the signal must be perceived in the presence of noise. If the pulse had not been smeared out, the eye would then integrate the noise only over the distance x_o. However, with the pulse smeared out, the eye would then integrate the noise

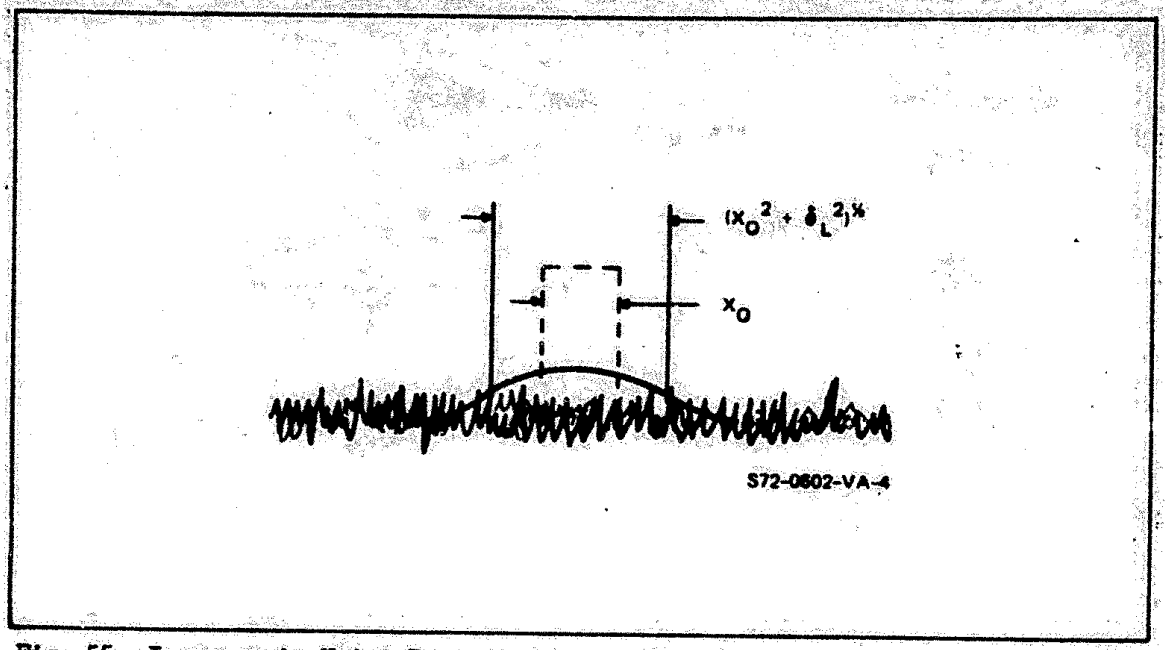

Fig. 55 Increase in Noise Perceived by an Observer due to an Increase in Effective Image Size due to an MTF Preceding a Point of Noise Insertion

over some larger distance; perhaps over an effective distance $(x_o^2 + \delta_L^2)^{\frac{1}{2}}$ as shown. Thus, while the aperture did not decrease the perceived signal, nor add noise of its own, it can increase perceived noise generated elsewhere in the imaging process. We note, for future reference, that the effect of noise added before an aperture is less serious than a noise added after an aperture for in the former case, the aperture also has a filtering effect on the noise.

In the treatment that follows, we shall consider the eye to be a perfect integrator in space. Assume a one-dimensional image with a white noise background of uniform variance $\hat{\sigma}^2$ units per cycle. The noise diagram is as shown in Fig. 56. For the noise model, we will assume the relation

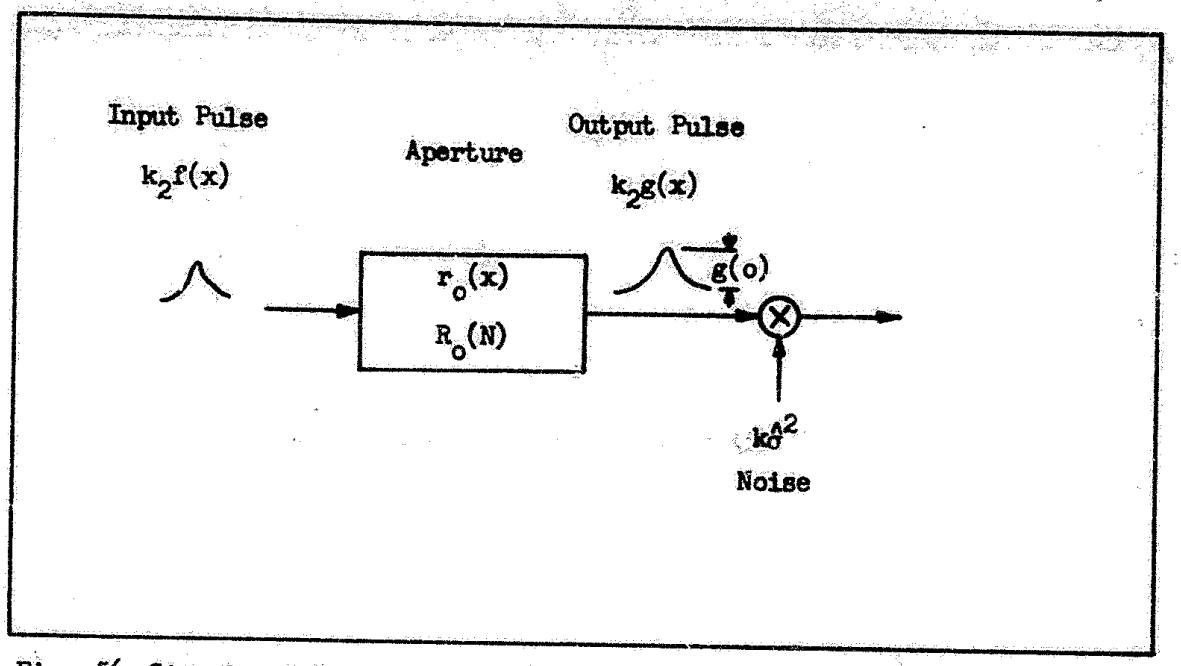

Fig. 56 Signal and Noise Diagram for the Case of an Aperiodic Image with Noise Added Subsequent to an Aperture.

$$\hat{n}_p^2 = (K\hat{G})^2 t \delta_o^2 \Delta B_N \tag{92}$$

where K is a unit conversion constant, t is the integration time of the eye, δ_o is the spatial duration of the image and ΔB_N is the noise equivalent spatial bandwidth. The duration variable, δ_o, expresses the notion that the eye integrates the image along the width of the image while ΔB_N expresses the notion that the noise is bandlimited. As will be seen, the output image waveshape itself determines both the duration and the bandwidth of the noise.

We define the duration variable to be the integral of the output image divided by the output pulse amplitude, i.e.,

$$\delta_o = \frac{k_2 \int_{-\infty}^{\infty} g(x)dx}{k_2 g(o)} = \frac{\int_{-\infty}^{\infty} g(x)dx}{g(o)} \tag{93}$$

With these results, we can write

$$\hat{n}_p^2 = (K\hat{\sigma})^2 t \frac{|F(o)|^2}{g(o)^2} \frac{\int_o^\infty |F(N)R_o(N)|^2 dN}{|F(o)|^2} \tag{94}$$

which can be simplified to

$$\hat{n}_p^2 = (K\hat{\sigma})^2 t \frac{\int_o^\infty |F(N)R_o(N)|^2 dN}{g(o)^2} \quad . \tag{95}$$

However, we shall use the previous form of Eq. (94) for illustrational purposes.

Suppose the input image is a rectangular image of the form given by Eq. (85) with $\alpha = 1$. When the input image width x_o is large with respect to δ_ℓ the noise equivalent line spread width of the aperture, and as previously noted in connection with Eq. (93),

$$\delta_o = \frac{F(o)}{g(o)} \quad . \tag{96}$$

The bandwidth ΔB_N is given by

$$\Delta B_N = \frac{\int_o^\infty |G(N)|^2 dN}{|G(o)|^2}$$

$$= \frac{\int_o^\infty |F(N)R_o(N)|^2 dN}{|F(o)|^2} \quad , \tag{97}$$

then $g(o) \tilde{=} 1.0$ and $F(o) \tilde{=} x_o$ as can be readily seen for the wide input pulse shown in Fig. 52. Also, $R_o(N)$ will be $\tilde{=} 1.0$ as can be seen for the spectrum of the wide pulse shown in Fig. 51. The result is that the duration variable becomes x_o and the bandwidth term becomes

$$\Delta B_N \simeq \int_0^\infty \frac{|F(N)|^2\, dN}{x_o^2} \quad . \tag{98}$$

For our unit amplitude rectangular pulse

$$F(N) = \frac{x_o \sin \pi N x_o/2}{\pi N x_o/2} \tag{99}$$

and

$$\int_0^\infty \frac{|F(N)|^2\, dN}{x_o^2} = \frac{x_o}{x_o^2} = x_o \quad . \tag{100}$$

Thus, $\Delta B_N = x_o$, and

$$\hat{n}_p^2 = (K\hat{\sigma})^2 t x_o^2 \cdot \frac{1}{x_o} \quad . \tag{101}$$

The root mean square noise becomes

$$\hat{n}_p = K\hat{\sigma}(x_o t)^{\frac{1}{2}} \tag{102}$$

which is seen to be simply proportional to the square root of the image area as the elementary model would lead us to believe.

For an intuitive feel for this result, we note once more that for images of large width, the duration of the image is the value of F(N) at N = 0 as shown in Fig. 51. The bandwidth is determined by normalizing F(N) by dividing by F(o) as shown in Fig. 57. Then the normalized function is squared and integrated to give the noise equivalent bandwidth ΔB_N as is also shown in the figure.

We next consider the case where the input image width becomes small with respect to the width δ_ℓ of the noise equivalent line spread

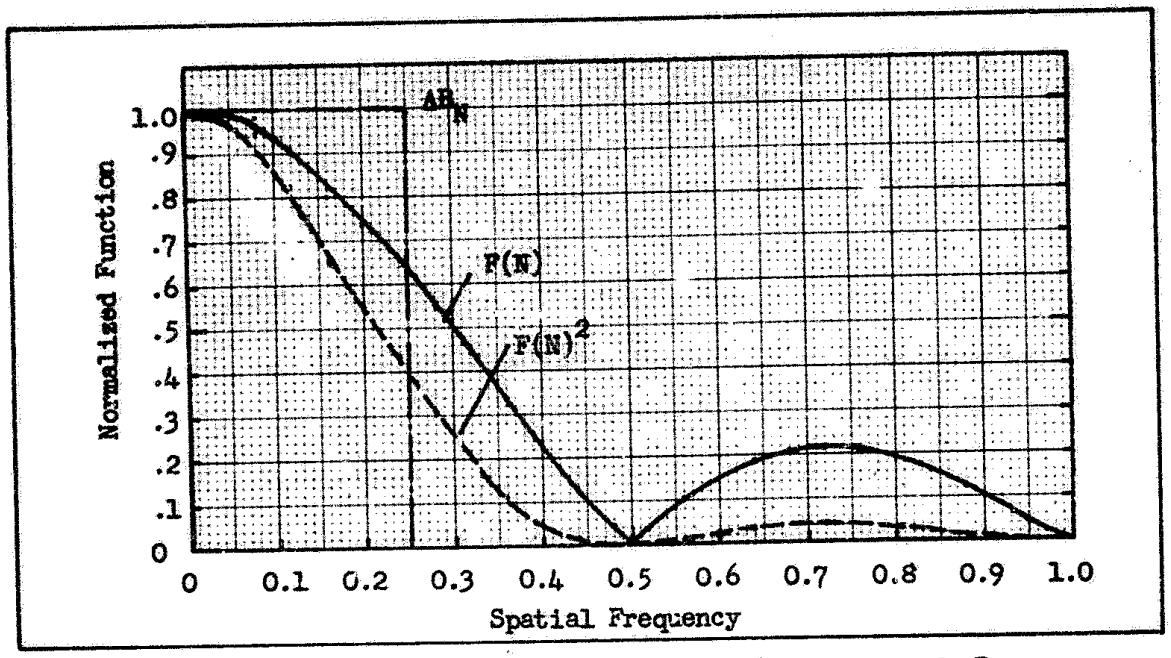

Fig. 57 Normalized Function F(N)/F(o) vs Spatial Frequency and ΔB_N the Noise Equivalent Bandwidth.

function. As the input image width approaches the dimensions of an impulse, F(N)/F(o) becomes numerically equal to unity (the Fourier spectrum of an impulse is a constant over all frequency). Therefore,

$$g(x) = F(0) \int_0^\infty \frac{F(N)}{F(o)} R_o(N) e^{j\pi N} \, dN$$

$$= x_o \int_0^\infty R_o(N) e^{j\pi N} \, dN$$

$$= x_o r_o(x) \tag{103}$$

That is, the output waveshape function takes on the shape of the aperture's impulse response. We observe that

$$g(o) = x_o r_o(o) \quad . \tag{104}$$

Using this result in Eq. (93),

$$\delta_o = \frac{F(o)}{g(o)} = \frac{x_o}{x_o r_o(o)}$$

$$= \frac{1}{r_o(o)} \quad . \tag{105}$$

Thus, the output image duration becomes a constant which is numerically equal to the inverse of the impulse response's amplitude.

This result may become somewhat clearer by noting that the equivalent impulse duration, δ_ℓ, as defined by a rectangle of amplitude equal to $r_o(o)$ and of width δ_ℓ selected so that $r_o(o) \cdot \delta_\ell$ is equal to the area under the impulse response, is numerically equal to

$$\delta_\ell = \frac{\int_{-\infty}^{\infty} r_o(x)dx}{r_o(o)} = \frac{1}{r_o(o)} \tag{106}$$

so that $\delta_o = \delta_\ell$ for the infinitesimally narrow input image.

As we noted above, $F(N)/F(o)$ becomes approximately unity as the input image width approaches an impulse. Hence, the noise equivalent bandwidth becomes simply

$$\Delta B_N = \int_o^N R_o^2(N)dN \tag{107}$$

which is numerically equal to Schades, N_e, the noise equivalent bandwidth, for an aperture. Then, the mean square noise becomes

$$\hat{n}_p^2 \simeq (K\hat{G})^2 t\delta_\ell^2 N_e \quad . \tag{108}$$

The noise equivalent bandwidth, N_e, is equal to

$$N_e = \frac{1}{\delta_e} \tag{109}$$

where δ_e is the noise equivalent aperture. Since δ_e is not far different from δ_ℓ, the rms noise becomes

$$\hat{n}_p \simeq (K\hat{\sigma})(t\delta_e)^{\frac{1}{2}} \tag{110}$$

and therefore, the rms noise is proportional to the square root of the noise equivalent aperture as the input image becomes very small.

Again, to develop an intuitive feel for this result, we note that for a small image, the output pulse spectrum assumes the form $x_o R_o(N)$. The noise equivalent bandwidth is determined by squaring $R_o(N)$ and integrating to give ΔB_N in a manner directly analogous to that used in obtaining ΔB_N of Fig. 57.

While the equations above for the limiting cases, (either very large or very small input images) are easy to use, many input images of interest fall between these extremes. To simplify the handling of these cases, we shall assume that both the input image and the aperture have Guassian waveshapes. Let the Fourier spectrum of the input pulse be

$$\frac{F(N)}{F(o)} = \exp - \frac{\pi}{8} \left(\frac{N}{N_{ex}}\right)^2 \tag{111}$$

and let the aperture's Fourier spectrum be

$$R_o(N) = \exp - \frac{\pi}{8} \left(\frac{N}{N_{e\ell}}\right)^2 \quad . \tag{112}$$

The noise equivalent bandwidth for the overall image is given by

$$N_{eo} = \int_0^\infty \frac{|F(N)R_o(N)|^2 dN}{F(o)^2}$$

$$= \int_0^\infty \exp - \left[\frac{\pi}{4} N^2 \left(\frac{1}{N_{ex}^2} + \frac{1}{N_{e\ell}^2}\right)\right] dN$$

$$= \frac{2}{\sqrt{\pi}} \frac{1}{\left[\frac{1}{N_{ex}^2} + \frac{1}{N_{e\ell}^2}\right]^{\frac{1}{2}}} \int_0^\infty \exp\theta^2 d\theta$$

$$= \frac{1}{\left[\frac{1}{N_{ex}^2} + \frac{1}{N_{e\ell}^2}\right]^{\frac{1}{2}}} \tag{113}$$

or

$$\frac{1}{N_{eo}} = \left[\frac{1}{N_{ex}^2} + \frac{1}{N_{e\ell}^2}\right]^{\frac{1}{2}} . \tag{114}$$

In terms of the noise equivalent apertures,

$$\delta_{eo}^2 = \delta_{ex}^2 + \delta_{e\ell}^2 . \tag{115}$$

For Guassian waveshapes, the overall noise equivalent aperture of a number of apertures in cascade can therefore be determined from the component apertures added in quadrature. Even when the input image waveshapes and

apertures are not Guassian, the approximation can be used with little error. If the input image is rectangular of duration, x_o, as in the examples above,

$$\delta_{eo}^2 = x_o^2 + \delta_{e\ell}^2 \quad . \tag{116}$$

A further approximation is that the duration variable, δ_o, of Eq. (91) above can also be approximated by δ_{eo}. Then,

$$\hat{n}_p^2 \simeq (K\hat{\sigma})^2 t\delta_{eo}^2 \cdot \frac{1}{\delta_{eo}} \tag{117}$$

and

$$\hat{n}_p \simeq K\hat{\sigma}(t\delta_{eo})^{\frac{1}{2}} \quad . \tag{118}$$

Now suppose first that the input wave shape is rectangular so that $\delta_{ex} = x_o$ and that the physical aperture, $\delta_{e\ell}$, is zero. Then,

$$\hat{n}_p \simeq K\hat{\sigma}(tx_o)^{\frac{1}{2}} \quad . \tag{119}$$

The ratio of Eq. (118) and the above, is designated the noise increase factor, ξ, i.e.,

$$\xi = \frac{\delta_{eo}}{x_o} = \frac{[x_o^2 + \delta_{e\ell}^2]^{\frac{1}{2}}}{x_o}$$

$$= [1 + (\frac{\delta_{e\ell}}{x_o})^2]^{\frac{1}{2}} \quad . \tag{120}$$

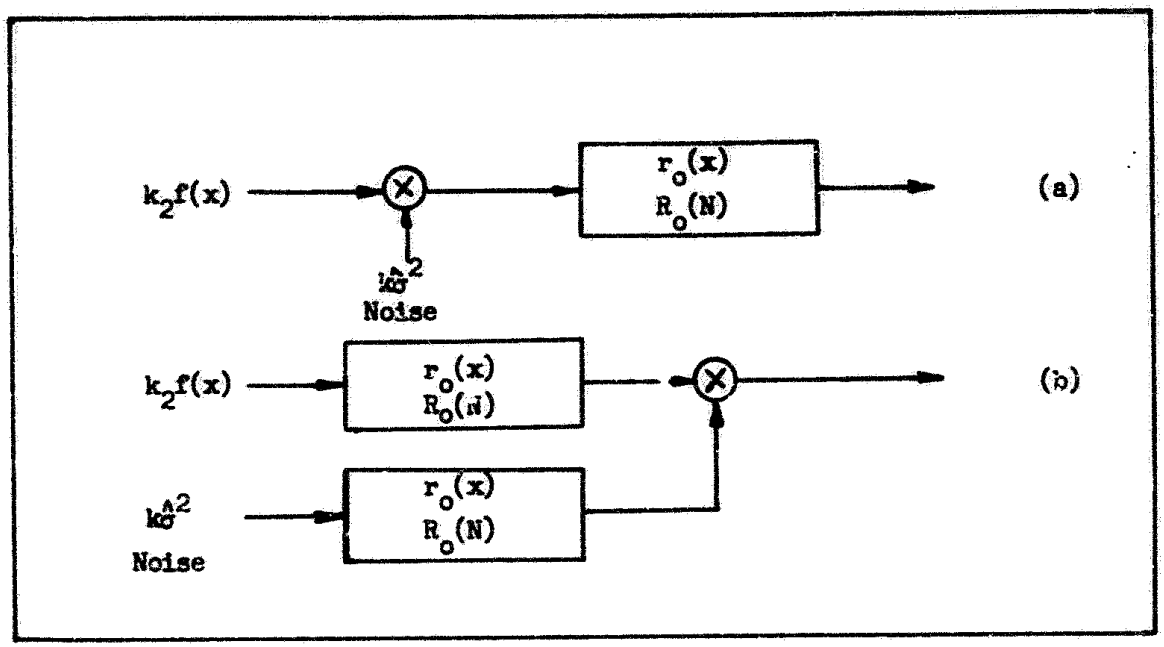

Fig. 58 (a) Aperture Following a Point of Noise Insertion, and
(b) Functional Noise Diagram for (a).

Using this noise increase factor, the Eq. (118) may be written as

$$\hat{n}_p = K\hat{\sigma}(t\xi x_o)^{\frac{1}{2}} \tag{121}$$

which will be a convenience in subsequent analyses.

We next consider the case where the aperture follows the point of noise insertion as shown in Fig. 58(a). In this case, the aperture function, $r_o(x)$, can both increase the perceived noise by increasing the noise integration distance and decrease it by virtue of a filtering action. In the previous case (noise added after the aperture), the

noise in the image is white in character (though spatially bandlimited). In the case now under consideration, the displayed noise will have a finite spectrum due to passing through the aperture.

Conceptually, the processes will be assumed to be of the following nature. The input image is first passed through the aperture so as to increase the noise integration distance. Next, the noise is band pass limited and added to the output signal as shown in the functional noise diagram of Fig. 58(b). For later convenience, we will first assume that the noise source follows the aperture in which case Eq. (91) above applies, i.e.,

$$\hat{n}_p^2 = (K\hat{\sigma})^2 t\delta_o^2 \Delta B_{NW} \tag{122}$$

except that the subscript W has been added to ΔB_N to indicate the white character of the noise. To correct for the finite noise spectrum, we write

$$\hat{n}_p^2 = (K\hat{\sigma})^2 t\delta_o^2 \Delta B_{NW} \cdot \frac{\Delta B_{NF}}{\Delta B_{NW}}$$

$$= [K\hat{\sigma}]^2 t\delta_o^2 \Gamma \Delta B_{NW} \tag{123}$$

where Γ is the correction factor for a finite noise spectrum. The noise bandwidth, ΔB_{NW}, is given by

$$\Delta B_{NF} = \int_0^\infty \frac{|G(N)R_o(N)|^2 dN}{F(o)^2}$$

$$= \int_0^\infty \frac{|F(N)R_o^2(N)|^2 dN}{F(o)^2} \quad . \tag{124}$$

Using the Guassian aperture approximation as in Eq. (115)

$$\delta_{eF} = [\delta_{ex}^2 + 2\delta_{e\ell}^2]^{\frac{1}{2}} \tag{125}$$

and since $\Delta B_{NF} = 1/\delta_{eF}$,

$$\Delta B_{NF} \simeq \frac{1}{[\delta_{ex}^2 + 2\delta_{e\ell}^2]^{\frac{1}{2}}} \quad . \tag{126}$$

Also,

$$\Delta B_{NW} = \frac{1}{[\delta_{ex}^2 + \delta_{e\ell}^2]^{\frac{1}{2}}} \tag{127}$$

so that the noise correction factor becomes

$$\Gamma = \frac{[\delta_{ex}^2 + \delta_{e\ell}^2]^{\frac{1}{2}}}{[\delta_{ex}^2 + 2\delta_{e\ell}^2]^{\frac{1}{2}}} \quad . \tag{128}$$

It is clear that Γ is a number less than one. Now,

$$\hat{n}_p^2 = (K\hat{\sigma})^2 t\delta_o^2 \Gamma \Delta B_{NW} \tag{129}$$

and by analogy to Eq. (121), we can write

$$\hat{n}_p = K\hat{\sigma}(t\xi\Gamma x_o)^{\frac{1}{2}} \quad . \tag{130}$$

The noise increase factor, ξ, is a number larger than one while the noise correction factor, Γ, is less than one. However, the product $\Gamma\xi$ is greater than one. Hence, the effect of an aperture following a point of noise insertion is to increase noise but by an amount less than if the aperture preceded the point of noise insertion.

Before continuing, we note that the general formulation for this case, corresponding to Eq. (99) for the previous case is given by

$$\hat{n}_p^2 = (K\hat{\sigma})^2 t \int_0^\infty \frac{|F(N)R_o^2(N)|^2 dN}{g(o)^2} \quad . \tag{131}$$

To complete this discussion, we consider the case of two apertures with two points of noise insertion, one noise following the first aperture but preceding the second and, the other noise at the output of the second aperture as shown in Fig. 59. To begin, we assume the two noises to be $\hat{n}_{p1}$ and $\hat{n}_{p2}$. If the apertures did not exist, then the two noise sources may be assumed to add in quadrature, i.e.,

$$\hat{n}_o^2 = \hat{n}_{p1}^2 + \hat{n}_{p2}^2 \quad . \tag{132}$$

If the input image is rectangular with duration x_o and if both noise sources are white, then

$$\hat{n}_o^2 = [(k_1\hat{\sigma}_1)^2 + (k_2\hat{\sigma}_2)^2]tx_o \quad . \tag{133}$$

Both apertures increase the noise integration distance by an amount ξ where

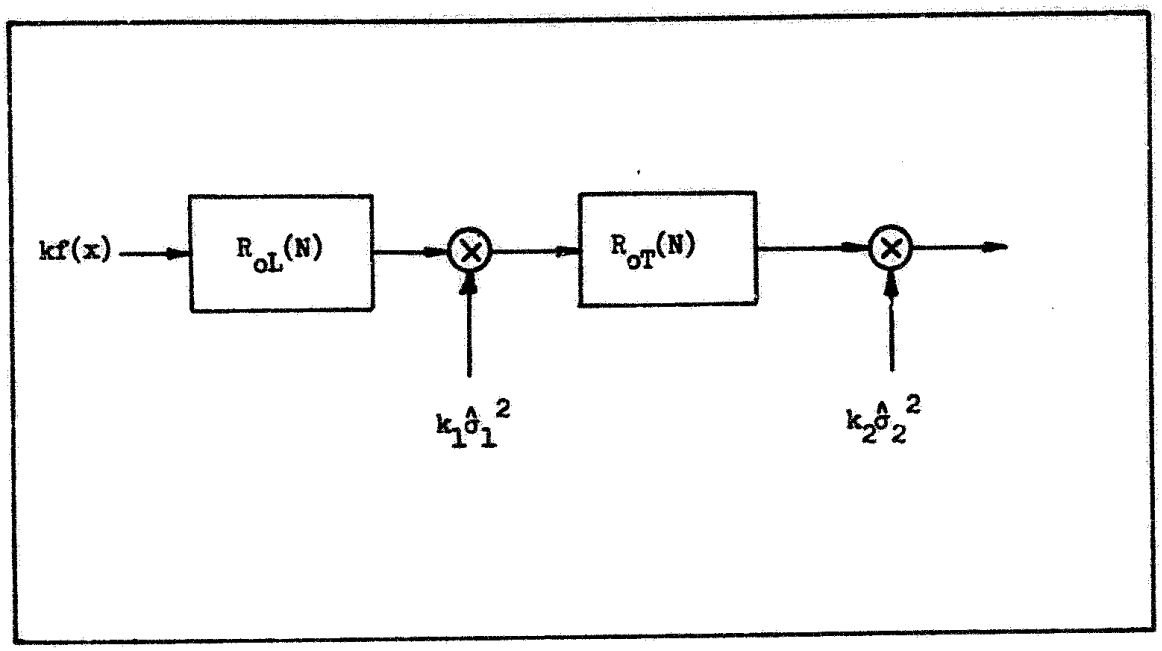

Fig. 59 Apertures Which Both Follow and Precede Points of Noise Insertion.

$$\xi = [1 + (\frac{\delta_{e\ell}}{x_o})^2 + (\frac{\delta_{eT}}{x_o})^2]^{\frac{1}{2}} \tag{134}$$

where $\delta_{e\ell}$ and δ_{eT} are the noise equivalent apertures of the first and second aperture respectively. Since the first noise source precedes the second aperture, the first noise must be corrected for a finite noise spectrum. The correction factor, Γ, is equal to

$$\Gamma = \frac{\xi_{xLT}}{[1 + (\frac{\delta_L}{x_o})^2 + 2(\frac{\delta_T}{x_o})^2]^{\frac{1}{2}}} \tag{135}$$

and the noise becomes

$$\hat{n}_o^2 = [(k_1\hat{\sigma}_1)^2\Gamma + (k_2\hat{\sigma}_2)^2]t\xi x_o \quad . \tag{136}$$

Both noises are increased by ξ, the noise increase factor, but, the noise which precedes the second aperture is filtered by it.

We turn next to the effect of apertures on periodic images. A one-dimensional pattern such as the conventional bar pattern is aperiodic along the bars and periodic in the direction transverse to the bars. Consequently, the analysis above applies along the bars but changes are needed in the periodic direction. If the input to a linear sensor is periodic, the output will also be periodic. The output and input periods (frequencies) will also be identical.

We suppose first that the MTF precedes the point of noise insertion. Then, the primary effect of the apertures will be to decrease the signal modulation. Since the period, or noise integration distance is unchanged (at least for the higher spatial frequencies) the perceived noise is unaltered as well. According to Schade, the mean signal associated with a bar pattern of spatial frequency N after the bar pattern has passed through an aperture of MTF, $R_o(N)$ is given in terms of a square wave flux response $R_{SF}(N)$ which is numerically equal to

$$R_{SF}(N) = \frac{8}{\pi^2} \sum_{k=1}^{\infty} \frac{|R_o(N)|}{k^2} \quad \text{for k odd.} \tag{137}$$

If the MTF precedes the point of noise insertion, the typical elementary SNR_D equation [see Eq. (4)] becomes

$$SNR_D = \left[\frac{t\epsilon}{\alpha}\right]^{\frac{1}{2}} \frac{R_{SF}(N)}{N} \frac{2C_M G i_{av}}{\left[eG^2 i_{av} + I_p^2/2\Delta f_v\right]^{\frac{1}{2}}} . \tag{138}$$

In the above, we have ignored the effect of the apertures along the length of the bars.

When the aperture follows a point of noise insertion, the aperture also filters the noise as it did in the aperiodic case. The noise filtering function for the periodic case is given by

$$\beta(N) = \frac{\int_0^N |R_o^2(N)|\, dN}{N} \quad . \tag{139}$$

This factor multiplies only the noises introduced prior to the location of the aperture. For example, the MTF of the sensor $|R_{oT}(N)|$ would usually filter the photoelectron noise of Eq. (139) but not the preamp noise. Then, Eq. (139) becomes

$$SNR_D = \left[\frac{t_i \epsilon}{\alpha}\right]^{\frac{1}{2}} \frac{R_{SF}(N)}{N} \frac{2C_M G i_{av}}{\left[eG^2\beta(N) i_{av} + I_p^2/2\Delta f_v\right]^{\frac{1}{2}}} \quad . \tag{140}$$

3.3 Effect of Apertures on Signal-to-Noise Ratio

We have derived and discussed the effect of finite sensor apertures on image waveforms and noise, in some detail. We now combine these effects with the elementary sensor model. For this purpose, we rewrite Eq. (64) below as

$$SNR_{DI} = \left[\frac{t_i \epsilon}{\alpha}\right]^{\frac{1}{2}} \frac{1}{N} \frac{2G_T C_M i_{av}}{\left[G_T^2 e i_{av} + I_p^2/2\Delta f_V\right]^{\frac{1}{2}}} \tag{141}$$

which was derived for a sensor with only two noise sources; photoelectron noise and preamp noise. A typical sensor of this type is shown

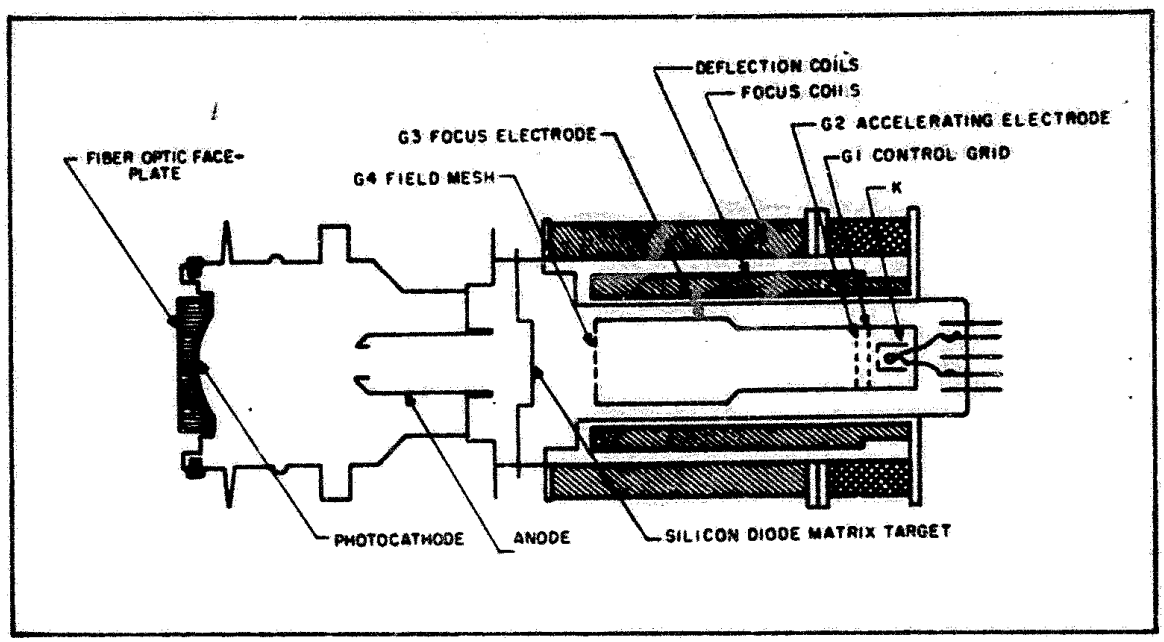

Fig. 60 Schematic of an EBSICON Camera Tube.

in Fig. 60. The lens represents an aperture preceding the point of photoelectron noise insertion (at the input photocathode) while the target follows the photoelectron noise input but precedes the preamp noise introduced at the target lead. The lens MTF is designated $R_{oL}(N)$ and the target MTF is $R_{oT}(N)$.

The effect of the apertures on an aperiodic object is to increase the noise leaving signal unchanged. The lens increases the perceived photoelectron and preamp noise as does the target, but the target also has filtering effect on the photoelectron noise. Quantitatively,

$$SNR_{DI} = \left[\frac{t_i \epsilon}{\alpha}\right]^{\frac{1}{2}} \frac{1}{[\xi_{xyLT}(N)]^{\frac{1}{2}} \cdot N} \cdot \frac{2G_T C_M i_{av}}{[G_T^2 e \Gamma_{xyT}(N) i_{av} + I_p^2/2\Delta f_V]^{\frac{1}{2}}} \quad (142)$$

where $\xi_{xy} = \xi_x \cdot \xi_y$ and ξ is given by Eq. (120) and $\Gamma_{xy} = \Gamma_x \cdot \Gamma_y$ and Γ is given by Eq. (128). For one-dimensional bar patterns, both the lens and target reduce signal modulation while the target has a filtering effect on noise. These effects are included in the equation below as

$$SNR_{DI} = \left[\frac{t_i e}{\alpha}\right]^{\frac{1}{2}} \cdot \frac{R_{SF}(N)}{[\xi_{yLT}(N)]^2 \cdot N} \cdot \frac{2G_T C_M i_{av}}{[G_T^2 e \Gamma_{yT}(N) i_{av} + I_D^2/2\Delta f_V]^{\frac{1}{2}}} \quad (143)$$

where $R_{SF}(N)$ is given by Eq. (139).

In this section, a theory of the effects of apertures on image detectability has been presented for stationary images. In the next section, the effects of image motion are included and in section 5, the preliminary attempts to verify the theory of apertures experimentally will be discussed.

4.0 Effects of Image Motion

Except when an object moves relative to a stationary background, relative scene/sensor motion is degrading to image quality. These degrading effects can be divided into three distinct mechanisms; the effect of the motion on the observer directly, the interaction of image motion and camera exposure time, and sensor time constant effects. These various effects were previously considered in Ref. 2 in some detail and will be further considered herein. In general, the effects of image motion on the observer are considered to be nearly negligible for the image motion rates commonly encountered in television practice. The interaction of image motion and exposure time is considered to be quite serious as can be discerned from the analytical treatment in Section 2 of this report. Also, sensor time constants can be limiting to system sensitivity and dynamic range.

In this section, motion experiments were performed to test the validity of certain of the image motion concepts and to gain further insight into the image motion problem. Specifically, psychophysical experiments were performed using moving bar patterns and the complex images (vehicles) used previously in the recognition experiments. The vidicon camera was used to generate the imagery. In these experiments, the light level was high enough so that sensor time constants are nearly negligible and the primary effect of motion is due to exposure time. Finally, further analysis was performed on sensor lag data previously taken for the purpose of improving the analytical sensor models.

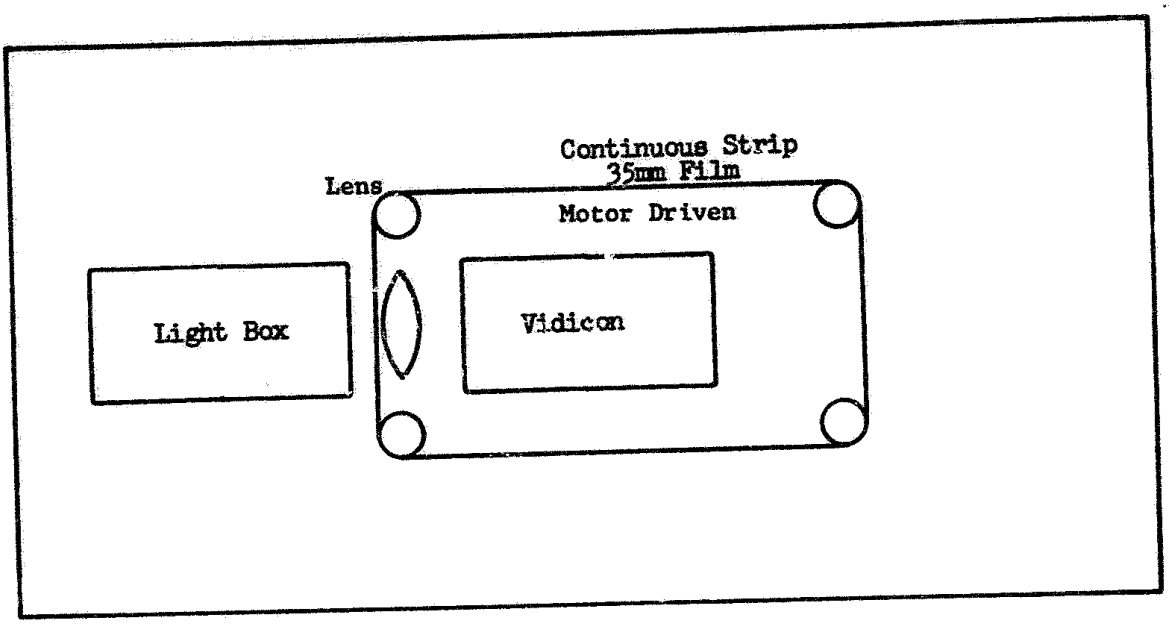

Fig. 61 Experimental Set Up for Motion Experiments

For bar patterns, the current motion MTF model was used (motion effects only--not lag), and it appears to be adequate for the particular case considered. For the vehicular imagery, an aperiodic model was applied with apparent success but the results must be considered tentative. The sensor-lag effects were and still are the most difficult to model although some correlations between observed image degradation and lag measurements are becoming apparent.

4.1 Psychophysical Experiments Involving Image Motion

The experimental set-up which was used for the motion experiments is shown in Fig. 61. A continuous strip of 35mm film was moved, at a constant speed, past the vidicon camera. Speed could be varied from less than 60 seconds per picture width to faster than 5 seconds per picture width. Motion could be either from left-to-right or right-to-left. For the experiments

with vehicle imagery reported here, a film speed of 10 seconds per picture width was used and the motion, as seen on the monitor, went from left to right. Four vehicle images were used, a tank, a van truck, a truck with a radar antenna on top and a mobile derrick with a bulldozer blade. The order of the images on the film was randomly chosen as was the signal-to-noise ratio of the image. Three observers participated in the experiment. A total of 600 data points were taken.

Display signal-to-noise ratio was calculated as follows. The broad area form of the SNR_D equation is used and for convenience it is repeated here as

$$SNR_{DI} = \left[2t\ \Delta f_V \frac{a}{K_d A}\right]^{\frac{1}{2}} SNR_V \qquad (144)$$

where $t = 0.1$, $\Delta f_V = 12.5 \times 10^6$ Hz and SNR_V is the peak-to-peak signal voltage (with image motion) in the image divided by the RMS noise voltage. The value of a/A that was used was the area of the image, a, on the photosurface divided by the active area of the photosurface, A, assuming a perfect lens with no MTF's effects. The factor of K_d in the equation comes from the assumption that we are to calculate SNR_{DI} of an equivalent bar pattern basis, that is, for recognition, the bars are each a/8 in area (see Fig. 3 of Section 2). In Table 6, the values of a/A and the unattenuated SNR_V values are listed for the images which were used in this experiment.

In Fig. 62, the calculated values of SNR_D are plotted as a function of corrected probability for the four images. The average SNR_{D-T} value, at the 50% probability level is 5.9. This is 80% higher than that which was obtained for the same targets when stationary.

Target	(a/A)	SNR_V (Zero db Level)
Tank	.000702	1
Derrick	.000514	.95
Truck	.000649	.80
Radar Truck	.000602	.90

Average a/A = .000615

Table 6 Values a/A and SNR_V Used for Motion Experiment

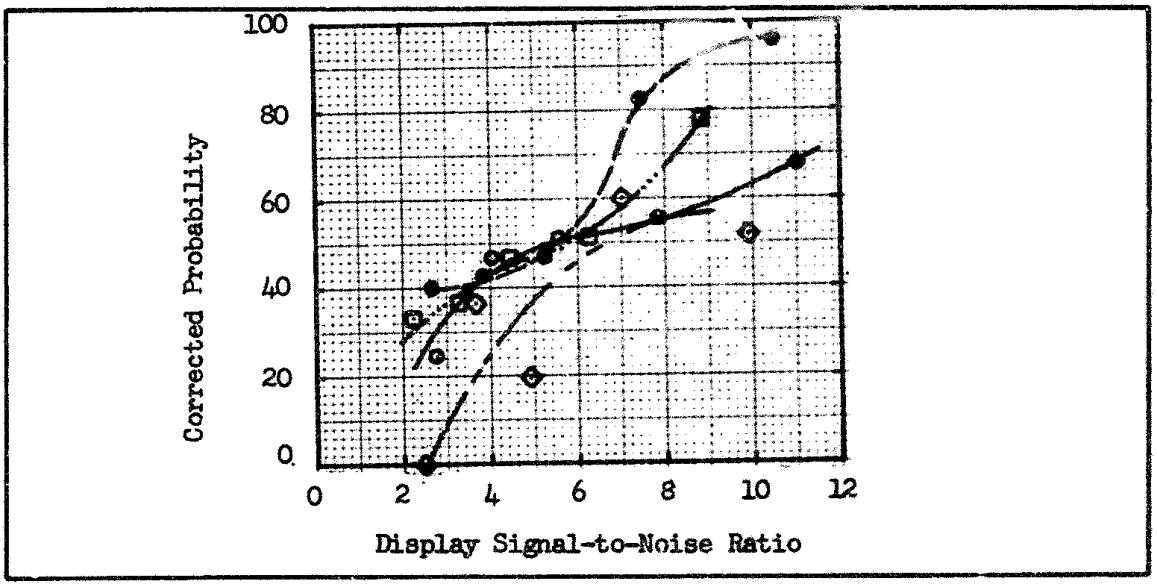

Fig. 62 Corrected Probability vs Display Signal-to-Noise Ratio for Target Recognition - Speed 10 Sec/Picture Height Tank ○ , Truck □ , Derrick ● , Radar Truck ◇ , Televised Images at 875 Lines, 25 frames/sec, $D_V/D_H = 3.5$

The above calculations ignored the MTF's associated with the lens, the camera, the interaction of camera exposure time and image motion. In the following these MTF's will be included in the SNR_{DI} calculation by using the aperiodic form of SNR_{DI} as developed in Section 3.

The aperiodic form of SNR_{DI} is

$$SNR_{DI} = \left[\frac{2t \quad \Delta f_v \; a}{\xi_{x_{LT}} \; \xi_{y_{LT}} \; K_d \; A}\right]^{\frac{1}{2}} SNR_V \tag{145}$$

where $\xi_{x_{LT}} \; \xi_{y_{LT}}$ account for the increase in the perceived noise due to the spreading of the image by the various MTF's. If the width of the actual image is x_o and the length is y_o, then $\xi_{x_{LT}} \; \xi_{y_{LT}}$ is given by

$$\xi_{x_{LT}} \cdot \xi_{y_{LT}} = \left[1 + \left(\frac{\delta_L}{x_o}\right)^2 + \left(\frac{\delta_T}{x_o}\right)^2 + \left(\frac{\delta_M}{x_o}\right)^2\right]^{\frac{1}{2}} \left[1 + \left(\frac{\delta_L}{y_o}\right)^2 + \left(\frac{\delta_T}{y_o}\right)^2\right]^{\frac{1}{2}} \tag{146}$$

where the subscripts L, T and M refer to the lens, camera tube, and motion respectively. The values of δ_L, δ_T and δ_M are calculated from

$$\delta_L = \frac{1}{N_{eL}} = \frac{1}{\int |R_{oL}|^2 \, dN} \tag{147}$$

$$\delta_T = \frac{1}{N_{eT}} = \frac{1}{\int |R_{oT}|^2 \, dN} \tag{148}$$

$$\delta_M = \frac{1}{\int |R_{oM}|^2 \, dN} \tag{149}$$

and the rest of the terms are as before.

In Table 7, the values of δ_L, δ_T, δ_M, x_o, y_o, $\xi_{x_{LT}}$, and $\xi_{y_{LT}}$ that are used for calculating Eq. (145) are listed. There was some vibration in our experimental set up due to the blower on the light box and an estimate of

Condition	Parameter						
	x_o	y_o	δ_L	δ_T	δ_M	$\xi_{x_{LT}}$	$\xi_{y_{LT}}$
Static	2.53×10^{-3}	4.05×10^{-2}	7.91×10^{-4}	4.11×10^{-3}	0	1.93	1.01
Motion	2.53×10^{-3}	4.05×10^{-2}	1.17×10^{-2}	4.11×10^{-3}	5.34×10^{-3}	5.43	1.05

Table 7 Parameters Used in Calculating SNR_n for Aperiodic Target

the overall MTF of the lens, including this vibration, was made from the static square wave response of the systems with the blower on. This data is shown in Figure 63.

Using the numbers from Table 7, we find that, statically $SNR_{D-T} = 2.2$ whereas dynamically $SNR_{D-T} = 2.5$. The two results are nearly the same and their difference is well within a reasonable experimental error.

To continue, we will show that the measured dynamic pattern square wave response is only slightly smaller than that obtained by multiplying the sensors static square wave response times the sine wave response for linear motion assuming complete sensor integration for one frame time (1/25 sec here). Assume that

$$R_{SQM}(N) = R_0(N)\, R_{SQ}(N) \tag{150}$$

where $R_{SQM}(N)$ is the dynamic square wave response, $R_{SQ}(N)$ the static square wave response of the sensor, and $R_0(N)$ is the sine wave response due to the interaction of linear motion and the sensor integration.

In reference (2), it was shown that the sine wave response due to the interaction of linear motion and sensor integration is given by

$$R_o(N) = \frac{\sin (\pi N v_i t_f/2Y)}{\pi N v_i t_f/2Y} \tag{151}$$

In laboratory measurements, it is the usual practice to specify the bar pattern velocity in terms of the number of seconds, t_s, required for one bar in the test pattern to traverse the long dimension of the field of view. Using this formulation, pattern velocity is

$$v_i = \frac{4}{3}\frac{Y}{t_s} \tag{152}$$

for our 4/3 aspect picture and Eq. (151) becomes

$$R_o(N) = \frac{\sin (2\pi N t_f/3t_s)}{2\pi N t_f/3t_s} \tag{153}$$

Eq. (153) is plotted in Fig. 63 as the circled points, o, and the measured static square wave response of the camera and lens is shown by the open squares, □ . The product of the two, Eq. (150), is shown by the solid circles, ●, in Fig. 64 and the measured dynamic square wave response is shown by the solid squares, ■ , in Fig. 64. As can be seen, the measured and the calculated results are nearly the same. For a given spatial frequency, the measured curve is about .80 times the calculated curve. It is believed that this discrepancy is due to the lag of the vidicon. Lag will be discussed further in the next section. The dynamic square wave pattern response of Eq. (150) is converted to a dynamic sine wave pattern response, R_{oM}, using Eq. (154), successively, starting at high line numbers where R_{SQM} is nearly zero and working down towards lower line numbers.

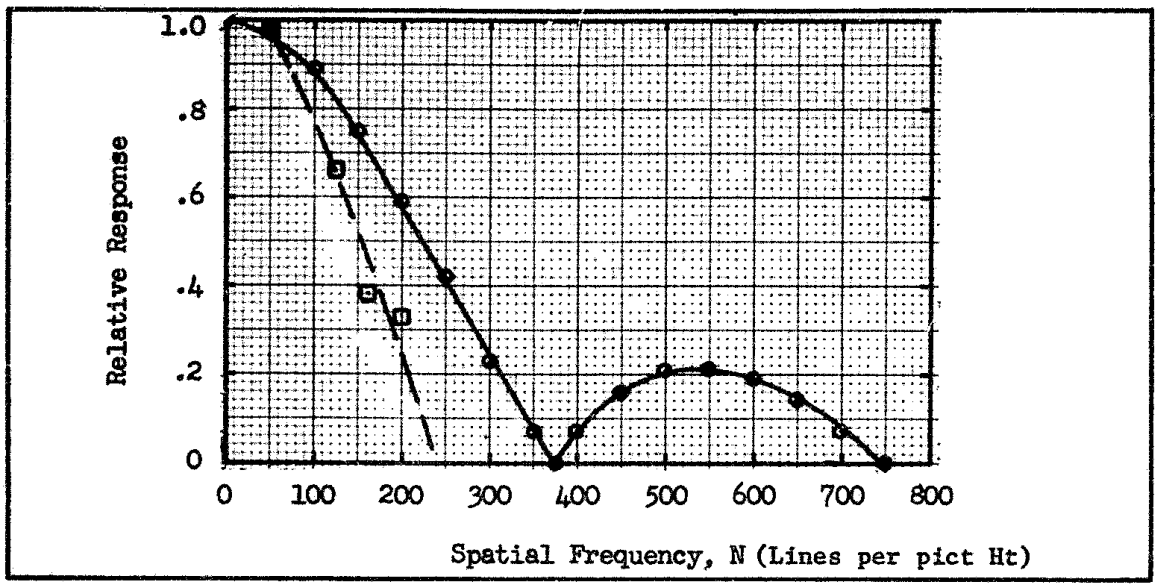

Fig. 63 Relative Response vs Spatial Frequency for Motion Experiment □ Static Case with Blower on, o Pure Motion, 10 Sec/Picture Height for a Frame Time 1/25 Sec.

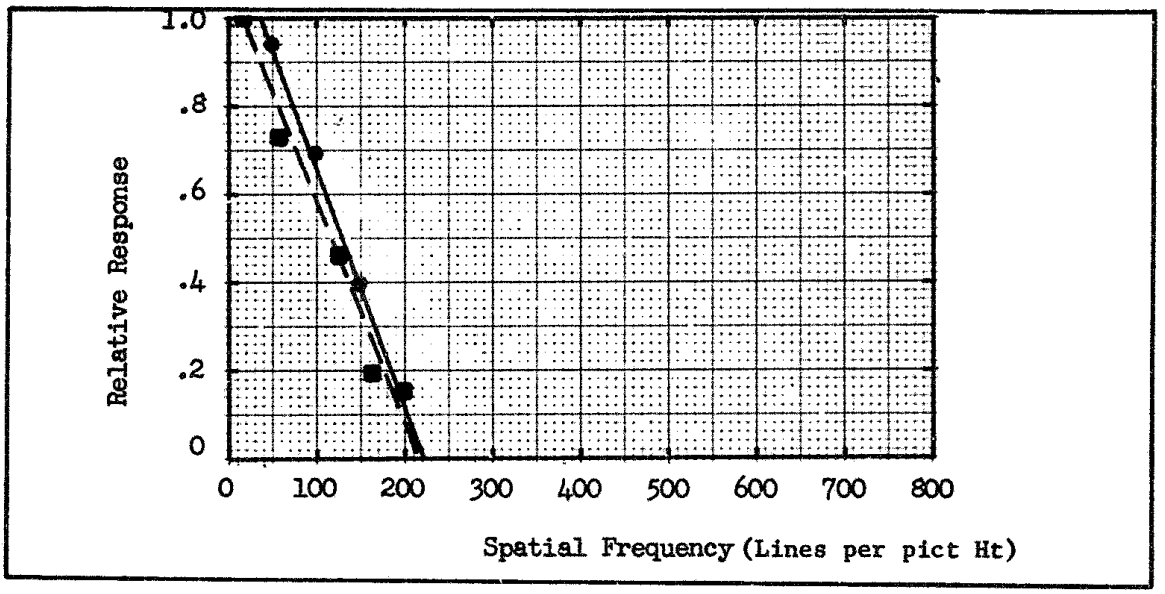

Fig. 64 Relative Response vs Spatial Frequency - Measured for 10 Sec/Picture Height ■ . Theoretical ●

$$R_{oM}(N) = \frac{4}{\pi}\left[R_{SQM}(N) - \frac{1}{3}R_{SQM}(3N) + \frac{1}{5}R_{SQM}(5N) \cdots\right] \quad (154)$$

In conclusion, it is seen that by including the MTF for sensor exposure time for linear motion and the effects of MTF of the sensor, as given by $\xi_{x_{LT}}$ and $\xi_{y_{LT}}$ in the SNR_{DI} calculation account nearly totally for motion effects when aperiodic targets are used. Further confirmation of this should be obtained using other speeds but, as of now, the concluaion seems reasonable and will be used. Of course, if the sensor had a great deal of lag, accounting for motion by the above method is inaccurate. More work remains to be done in this area.

4.2 Analysis of Sensor Motion Data

It was seen in the last section that the dynamic square wave response of the laboratory vidicon which was used for the psychophysical experiments was only slightly lower than that predicted by the product of the vidicon's static square wave response and the MTF that is characteristic of an ideal integrating surface. It is of interest to investigate whether such a simple result can be extended to other camera tubes as well. In the following, experimental results confirm that this model can be used for resistive sea silicon diode targeted tubes such as the EBS if the tube is operated at high target voltages (low lag) but the results are seen to be extremely optimistic if the target is operated at low voltages (high lag).

The analysis which follows is an extension of that which was reported in Ref. (2). The measurements were made on a Westinghouse WX-31841 camera tube operated at high (20 volts) and low (7.5 volts) target voltages. At the high target voltage, camera lag is small whereas at low target voltage,

camera lag is high. This tube employs a 40 mm diameter photocathode of the multialkali type, a minifying diode electrostatic image section and a resistive sea type silicon diode array target of 25 mm active diameter with 2,000 diodes per linear inch. The readout beam is magnetically focussed and deflected. The picture aspect ratio was 4/3 (width-to-height). Measurements were made under standard TV scan conditions utilizing two interlaced fields per frame. The preamplifier noise was approximately 12 nA (rms) at a bandwidth of 12 MHz. Measurements were made of the static square wave response, of dynamic square wave response using a moving resolution test chart, of buildup and decay lag, and of the static and dynamic limiting resolution.

Dynamic amplitude response measurements were obtained by imaging a slant burst pattern from an RCA P-200 resolution test chart onto the tube photocathode. The pattern was affixed to a continuous transparent belt that could be run at various speeds across the field of view of the camera tube. The pattern was illuminated from behind and the image adjusted to the proper size. The illumination was adjusted to give a static signal current (in excess of the dark current) of 400nA. The signal modulation of the line bursts was displayed on an oscilloscope and the percent modulation was read directly from the oscilloscope presentation. With this chart, a bandwidth of only 4 MHz was required which resulted in a significant decrease in noise and allowed the direct reading of the oscilloscope with a reasonable accuracy for chart speeds as high as 2.5 seconds per picture width.

Because of the test chart design, it was found necessary to adjust the chart speed for each resolution line number in order to obtain an equivalent single speed corresponding to that which would have been used with a vertical bar chart. Chart speeds were employed that gave equivalent vertical

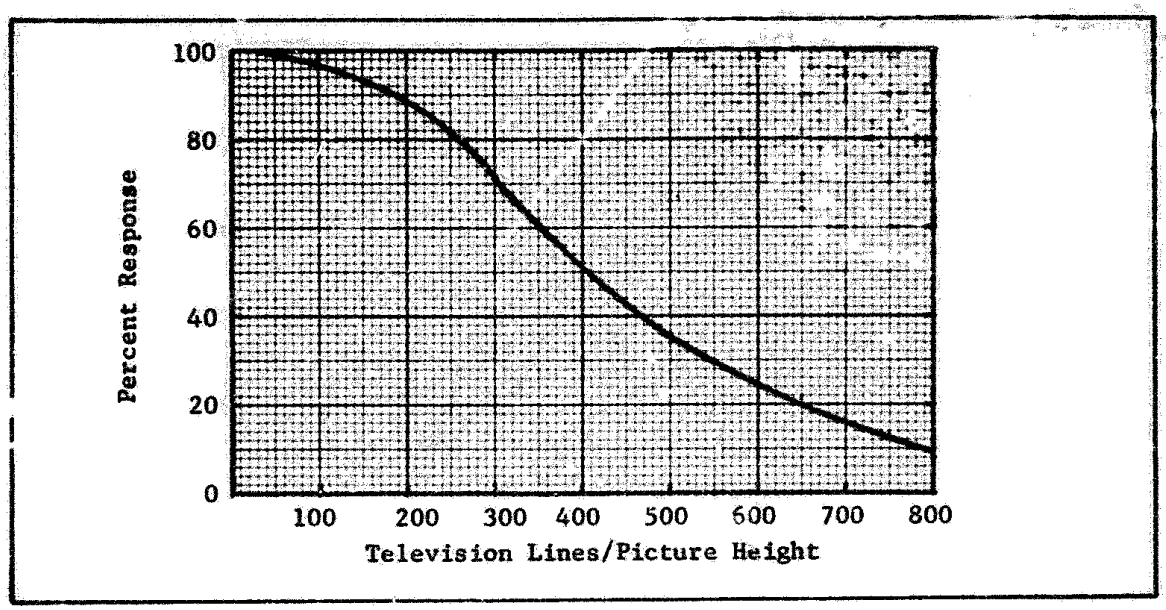

Fig. 65 Static Amplitude Response for WX31841

bar chart speeds of 60 sec/picture width, 20 sec/picture width and 10 sec/picture width. Measurements were made at target voltages of V_T = 20 volts and 7.5 volts for resolution line bursts of 100, 200, 400, and 600 TVL per Raster Height.

In Fig. 65, the static square wave response is shown and in Figs. 66, 67, and 68, the dynamic square wave response are shown. Also indicated in the figures are the theoretical curves which were obtained by multiplication of the static square wave response and the motion MTF. For a target voltage of V_T = 20 volts, the low lag case (3rd field signal is≈19%), the measured data and calculated data are similar for chart speeds of 10 and 20 seconds per picture width (the average difference is 24%), and for 60 seconds, the measured results are within an average of 8% of the predicted numbers. With a target voltage of V_T = 7.5 volts, the high lag case (3rd field current is

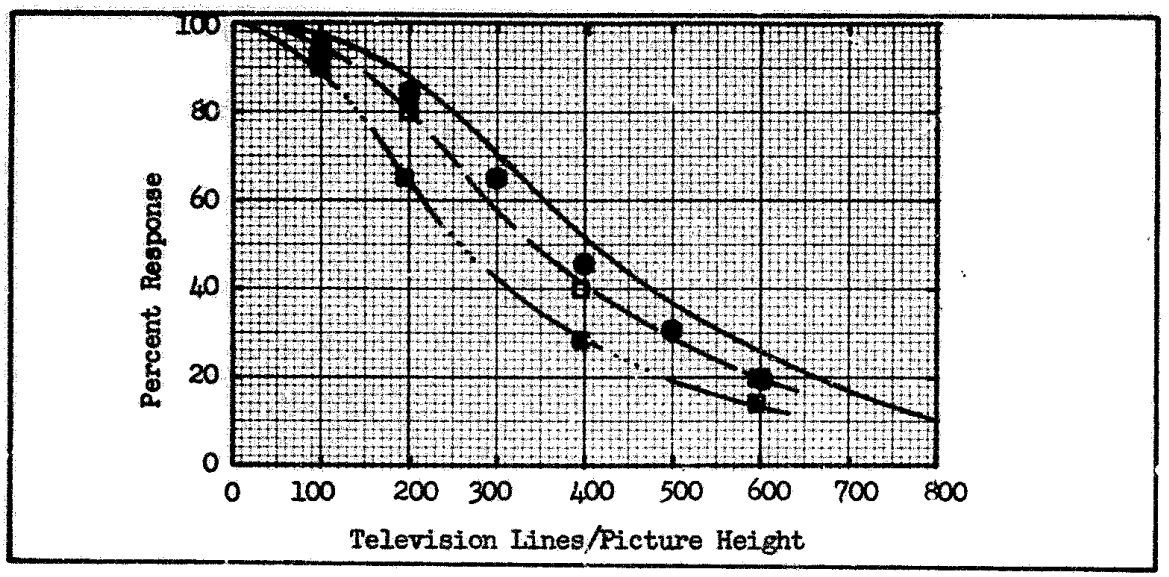

Fig. 66 Dynamic Amplitude Response for Pattern Speed of 60 Second/ Picture Width □ V_T = 20V, ■V_T = 7.5V for WX 31841 - Solid Curve Static Case ● Theoretical

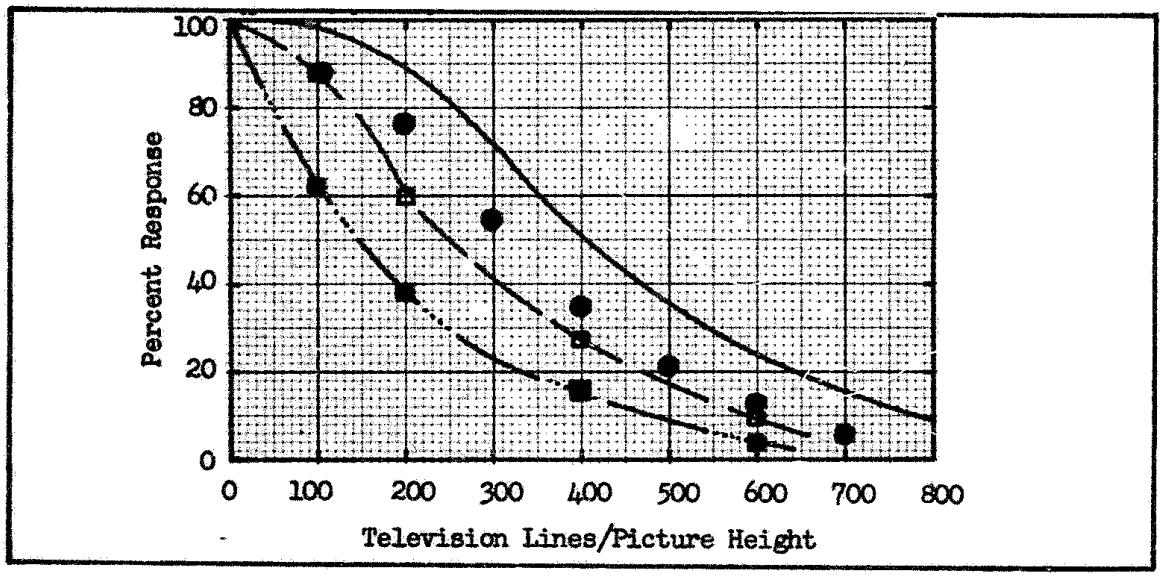

Fig. 67 Dynamic Amplitude Response for Pattern Speed of 20 Seconds/ Picture Width □ V_T = 20V, ■V_T = 7.5V for WX 31841 - Solid Curve Static Case ● Theoretical

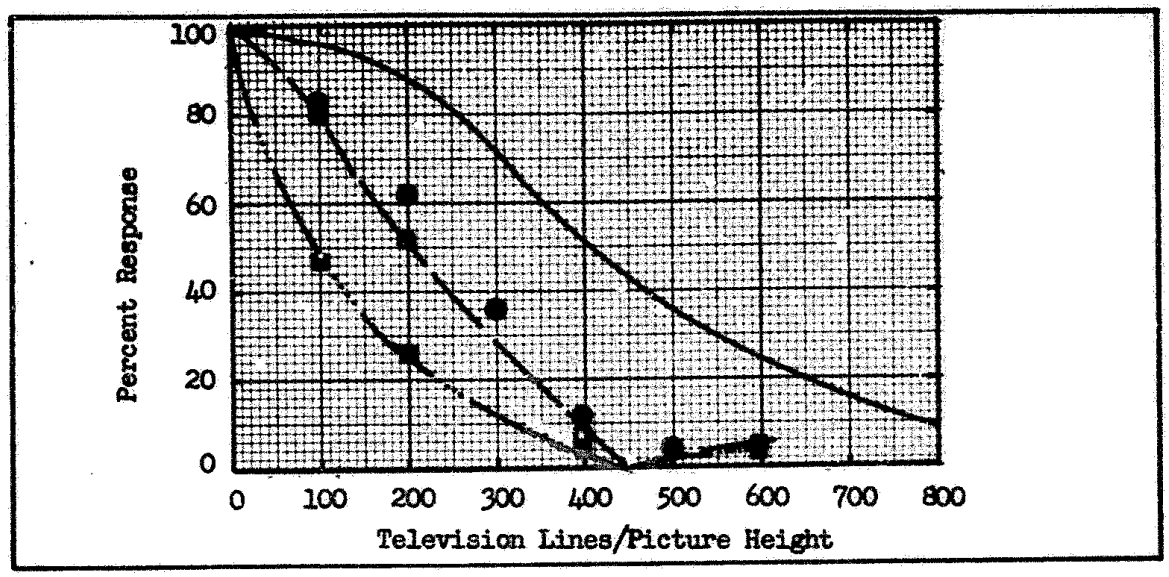

Fig. 68 Dynamic Amplitude Response for Pattern Speed of 10 Seconds/Picture Width □ V_T = 20V, ■ V_T = 7.5V for WX 31841 - Solid Curve Static Case ● Theoretical

≈47%), the measured result is on the average 49% smaller than the calculated; the difference is the largest for the fastest target speed.

Plots of the buildup and decay values are shown in Fig. 69. To within the experimental accuracy the sum of the two values at a given target voltage is unity. If γ is the fraction of charge neutralized during one readout, then as is shown in Ref. (2), the buildup lag = $\gamma(5 - \gamma)/4$ and the decay lag = $(4 - \gamma)(1 - \gamma)/4$. In Fig. 70, a plot of γ is shown as a function of target voltage which was obtained for buildup lag using the data from Ref. (2). From Fig. 70, it is seen that $\gamma \approx \ln V_T$.

For the above, the buildup and decay lag are defined as follows. A small spot of light is imaged onto the center of the input to the camera tube and the resulting signal current as a series of pulses, one for each successive field, is displayed on an oscilloscope. The occurrence of a

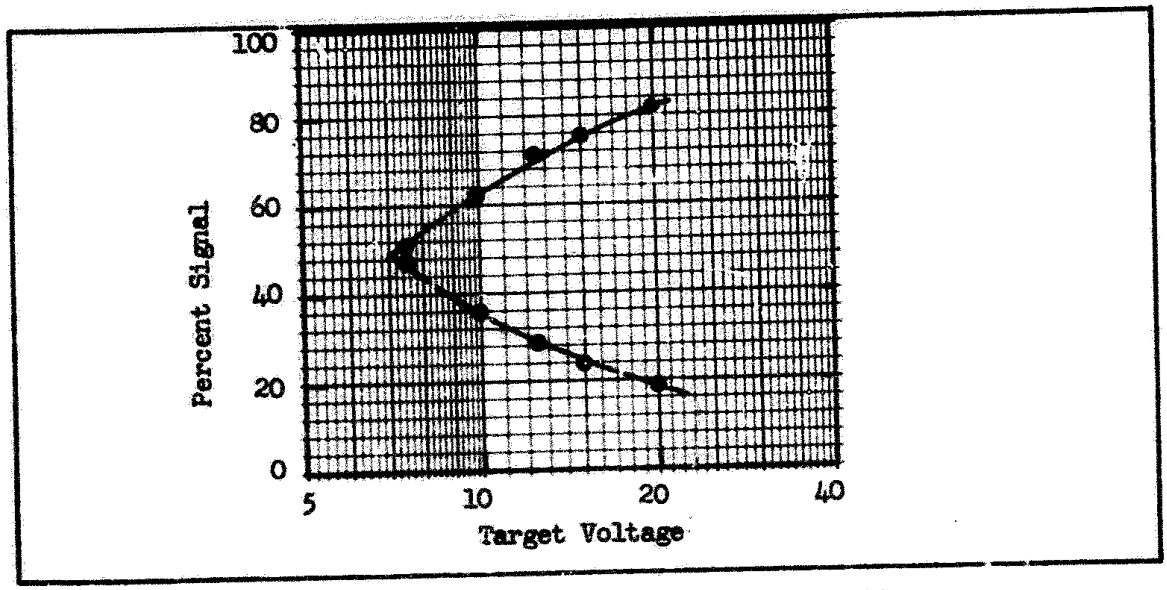

Fig. 69 Build Up Lag ● , Decay Lag ○ As a Function of Target Voltage for WX 31911

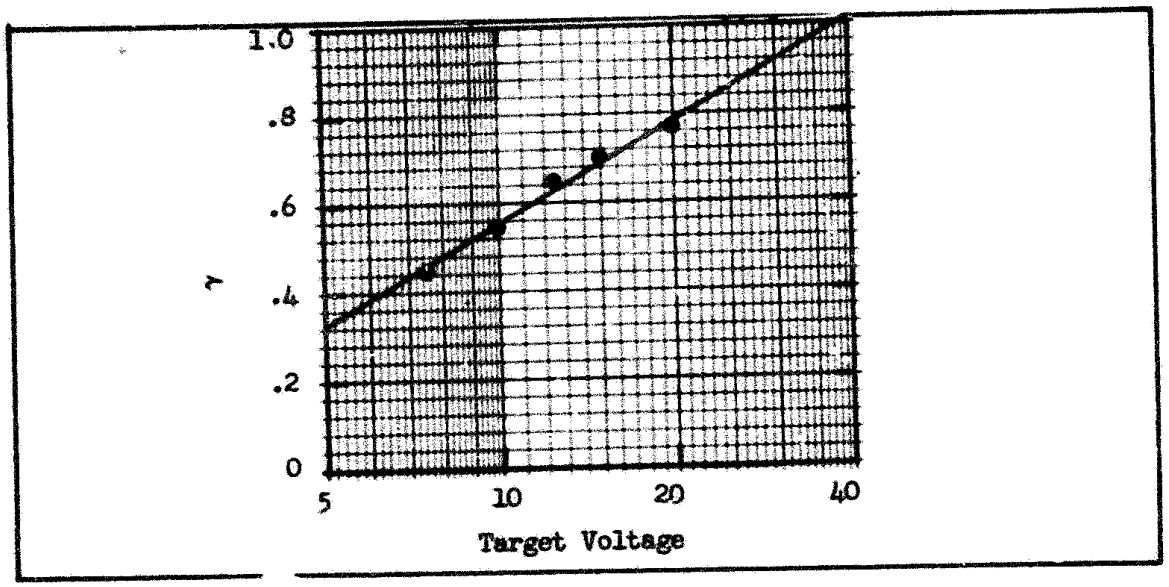

Fig. 70 Gamma, . for Different Target Voltages for WX 31911

pulse is mid-time between the beginning and end of any field. This time is given a field designation. At the same time during a vertical flyback the illumination is turned on. The field prior to this is designated zero and that following the onset of illumination is denoted one. Thus, the illumination is turned on mid-time between the zero and first field readouts. The light remains on for a sufficient number of fields to permit a steady state to occur and then mid-time between two successive field readouts the illumination is removed for an equal number of fields. The build up lag is defined as the ratio of the third field current (after turn on of the light) to the steady state value times 100 and the decay lag is defined as the ratio of the third field current (after turn off of the light) to the steady state value times 100.

Similar to the measurement of dynamic amplitude response, measurements were made of the tube dynamic limiting resolution by imaging a 100% contrast Westinghouse vertical bar resolution chart on the camera tube and determining the minimum illumination required to permit perception of various resolution line numbers. For these tests the tube was operated with target voltages of 7.5 and 20 volts with the chart stationary and moving at speeds of 60, 20, 10 and 5 seconds per picture width. All measurements were made with a photocathode potential of -10Kv and a video bandwidth of 12 MHz. From the resulting data, curves of limiting resolution as a function of photocathode illumination for the various rates of image motion were generated. These are presented in Fig. 71 for a target voltage of 20 volts and Fig. 72 for a target voltage of 7.5 volts.

Curves similar to those shown in Figs. 71 and 72 were generated using 35% contrast patterns and are shown in Figs. 73 and 74. One image speed

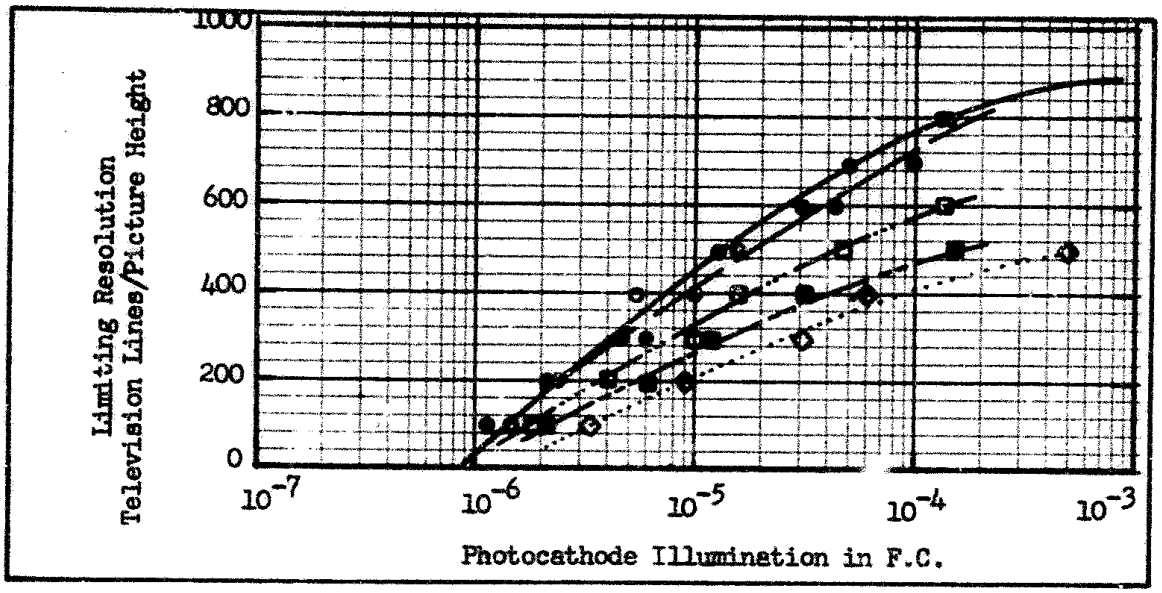

Fig. 71 Dynamic Sensitivity for 100% Contrast Pattern, V_m = 20 volts ○ Static, ● 60 Sec/P.W., □ 20 Sec/P.W., ■ 10 Sec/P.W., ◇ 5 Sec/P.W., Bandwidtn 12Mhz

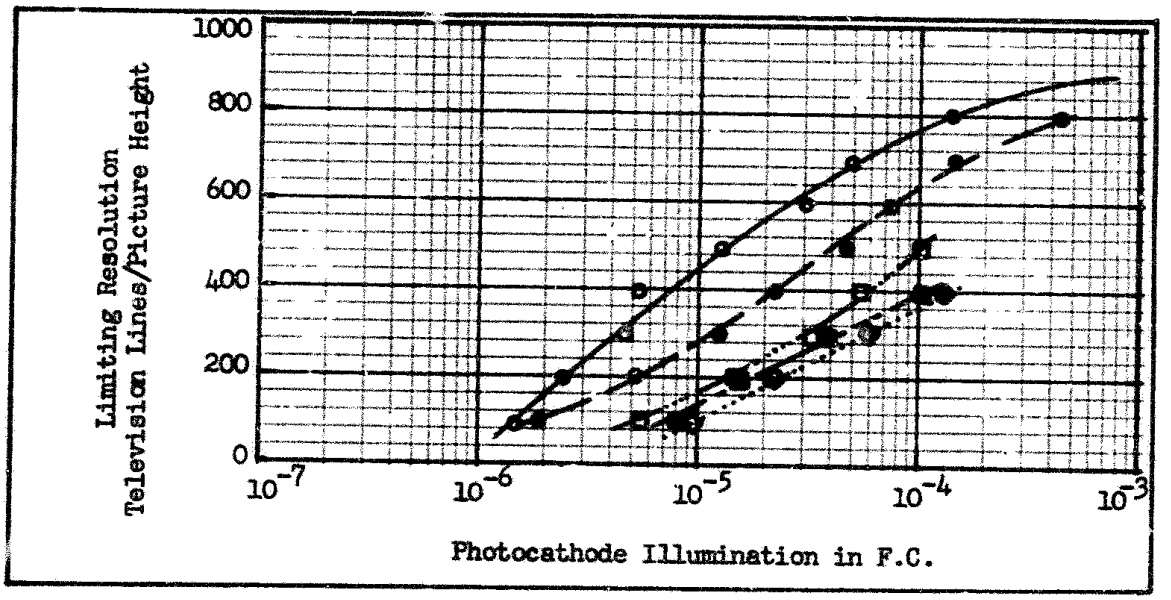

Fig. 72 Dynamic Sensitivity for 100% Contrast Pattern, V_m = 7.5 volts ○ Static, ● 60 Sec/P.W., □ 20 Sec/P.W., ■ 10 Sec/P.W., ◇ 5 Sec/P.W., Bandwidth 12 Mhz

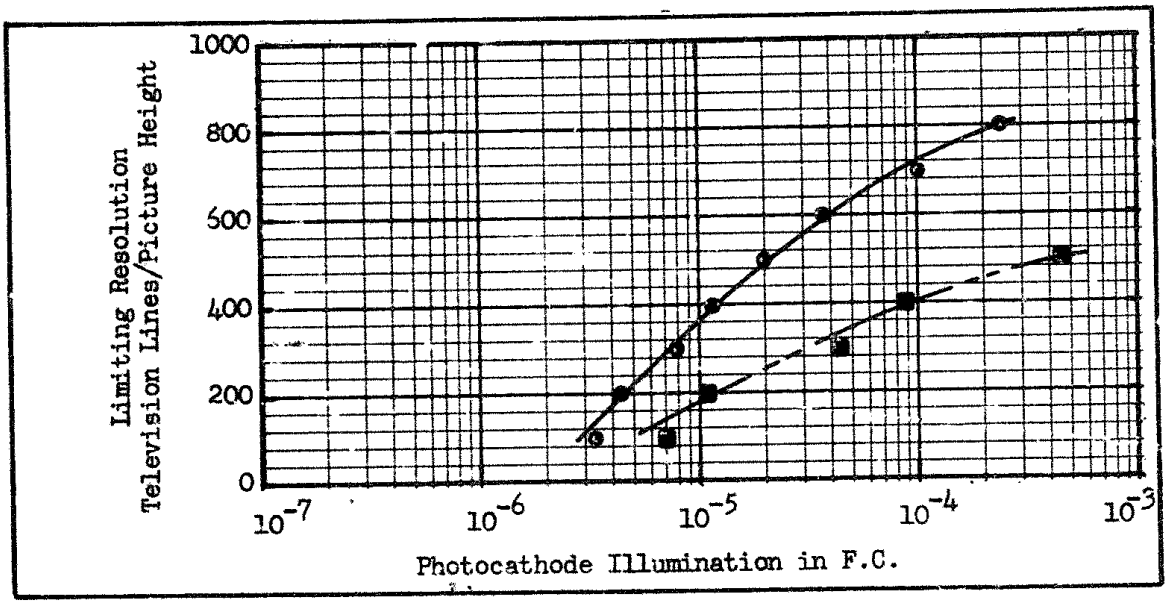

Fig. 73 Dynamic Sensitivity for 35% Contrast Pattern, V_T = 20 volts
o Static, ■ 10 Sec/P.W., Bandwidth 12 MHz

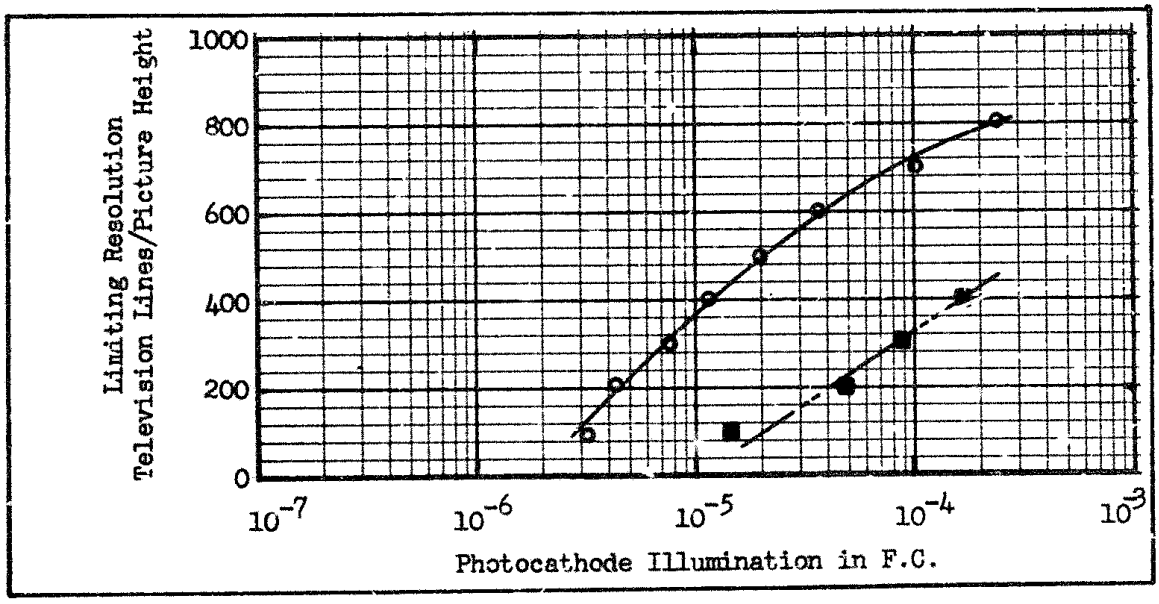

Fig. 74 Dynamic Sensitivity for 35% Contrast Pattern V_T = 7.5 volts
o Static, ■ 10 Sec/P.W., Bandwidth 12 MHz

was used, 10 seconds per picture width and the two target voltages used were 20 and 7.5 volts. For each target voltage with the 35% contrast pattern, the loss in sensitivity due to motion is approximately the same as that measured for the same speed with the 100% contrast pattern.

Assume that the threshold SNR_{D-T}, for the low lag situation is a constant, independent of pattern speed. Then, for a given pattern speed, the increase in light level that is required for a given line number should be inversely proportional to the dynamic flux factor. Let the pattern speed be v and the line number N. Statically, the required light level is E_S and dynamically, the required light level is E_{vS}. If the static flux factor is $R_{SF}(N)$ and the dynamic flux factor $R_{vSF}(N)$ then, if linear motion alone accounts for the charge in light level, we have that

$$\frac{R_{vSF}(N)}{R_{SF}(N)} = \frac{E_S}{E_{vS}} \tag{155}$$

For the calculation of $R_{SF}(N)$ and $R_{vSF}(N)$, the static and dynamic sine wave response is used, respectively. The dynamic sine wave response is calculated from the dynamic square wave response as discussed above. Our assumption of constant SNR_{D-T}, independent of pattern velocity is found to be only approximately true. The departures are the largest at high line number and high pattern speeds, and increases in E_S of a factor of 2 larger than that expected by Eq. (155) are found. The results are further off for the high lag case, an added increase in the photocathode illumination from 2 to 3 times over that used for the low lag case were found. Thus for high lag, discrepancies (increases) as high as a factor of 5 or more greater than that expected from just linear motion and sensor integration are required.

5.0 Psychophysical Experiments Involving Sensor MTF

In most of the previous psychophysical experiments, the effects of sensory system MTF's were avoided by using electronically generated imagery or a high resolution TV camera and, test images whose details were large enough to preclude serious image smearing effects. In Section 3, we discussed general theories concerning the effects of sensor MTF's on periodic and aperiodic test objects. While the theory is believed to be sound and has been shown to account for most of the first order effects observed experimentally, specific psychophysical experiments have not been performed in the past to verify the theory in detail. It should be observed that certain of the effects are not strong variables and because of the statistical nature of the psychophysical experiments, difficulty in verifying the theory with high confidence may be expected. However, the experiments performed and discussed herein do tend to confirm the general theory.

The experimental set-up of Fig. 75 was used to perform the psychophysical experiments. The test images are projected on the faceplate of a high resolution 1-1/2" vidicon operated at highlight video signal-to-noise ratios of 50:1 or better. The camera and TV monitor were operated at 25 frames/second with 875 scanning lines (825 active). Band-limited white noise of Guassian distribution was mixed with the camera generated signals. Both the signals and noise were passed through identical filters (noise equivalent bandwidth of 12.5 MHz) prior to mixing in the monitor. The monitor luminance was approximately 1 ft. Lambert unless otherwise specified. The displayed picture height was 8" and the observer-display distance was 28".

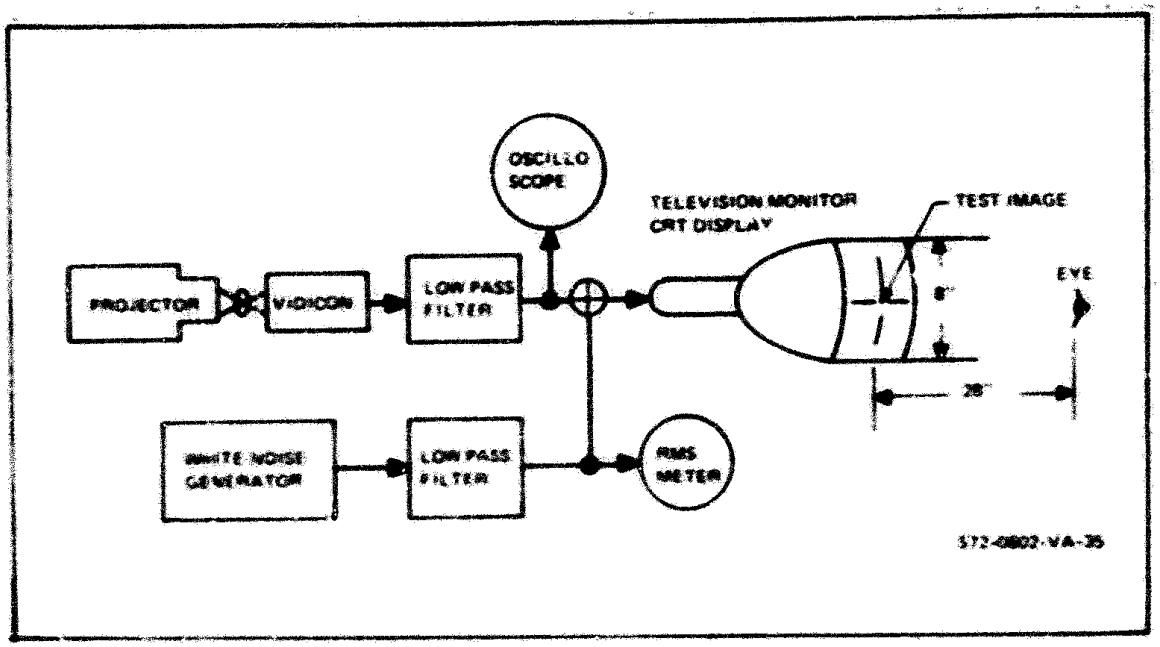

Fig. 75 Experimental Set-up for the Television Camera Generated Imagery

The MTF of the set-up (vidicon and lens) was changed by defocusing the lens. In Fig. 76 the overall MTF's that corresponded to three experimental conditions are shown. For Case A, the lens was in focus, for Case B, the lens is somewhat out of focus, and for Case C, the lens is very much out of focus. The values of N_{eT} and N_{eL}, for the three cases are listed in Table 8 where N_{eT} and N_{eL} are calculated from Eqs. (5 and 6). N_{eLT} is the overall N_e as calculated from Fig. 76.

Most of the experiments were performed using the MTF of either Case A or Case C. The method of limits described in Ref. (2) was used to take the data. The camera viewed a transparency which contained a number of patterns of different frequency. The video signal-to-noise ratios were systematically varied in 1 db steps up and down, and at each step the subject

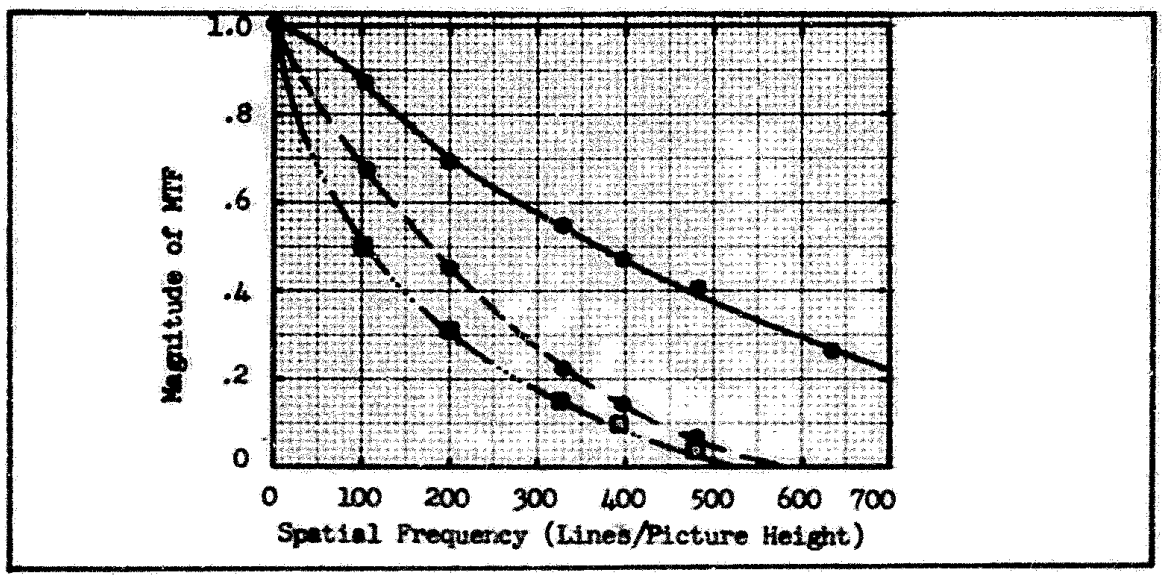

Fig. 76 Modulation Transfer Functions for Case A ● , Case B ○ , and Case C □ - Lens and Camera Combined

Case	N_{eT}	N_{eL}	N_{eLT}
A	261	1266	252
B	261	123	110
C	261	72	69

Table 8 Value of N_{eT} and N_{eL} and Overall N_{eLT} for Three Cases

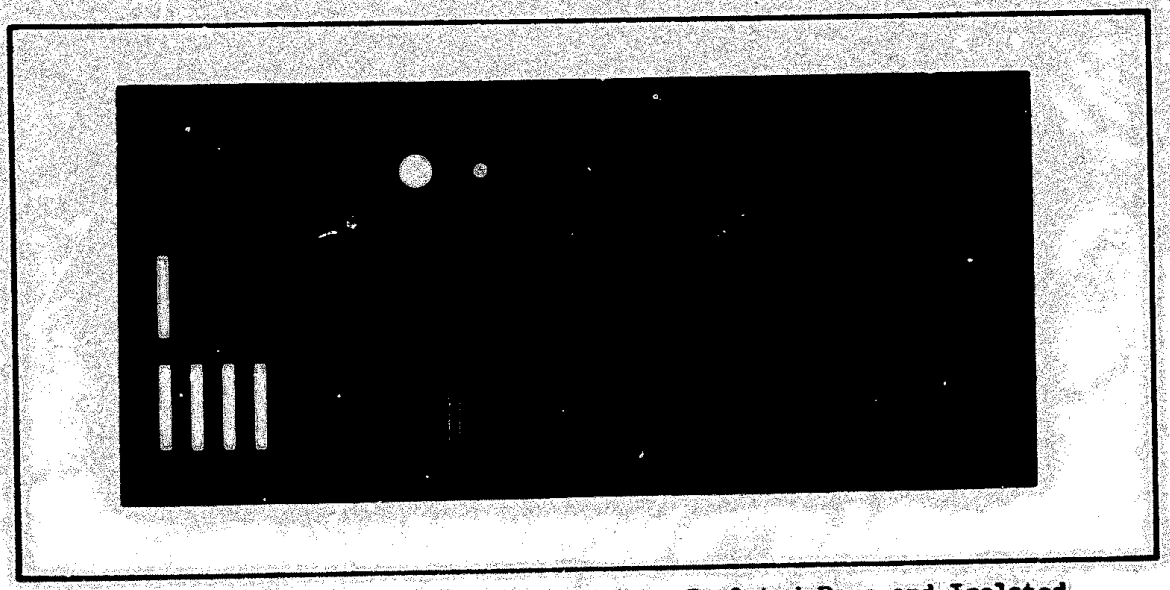

Fig. 77 Bar Patterns of Variable Aspect, Isolated Bars and Isolated Circles Used for Experiments

was required to specify the highest frequency pattern which could be barely resolved. Four different images were used, isolated circles, isolated bars, bar patterns of variable aspect, and bar patterns of constant aspect (5:1). A photograph of the isolated circles, isolated bars and bar patterns of variable aspect is shown in Fig. 77 and in Fig. 78 a photograph of the constant aspect bar patterns is shown. Table 9 lists the line number, N, for the various images calculated from

$$N = \left(\frac{H}{x_o}\right) = \frac{Y}{\Delta x} \tag{156}$$

where H is the effective height of the transparency (that which is projected onto the photocathode of height .6 $D_{pc} = Y$ where D_{pc} is the photocathode diameter) and x_o is the width of a bar. Δx is the bar width on the photocathode. Also listed in Table 9 is the bar length/width ratio, n_v. For

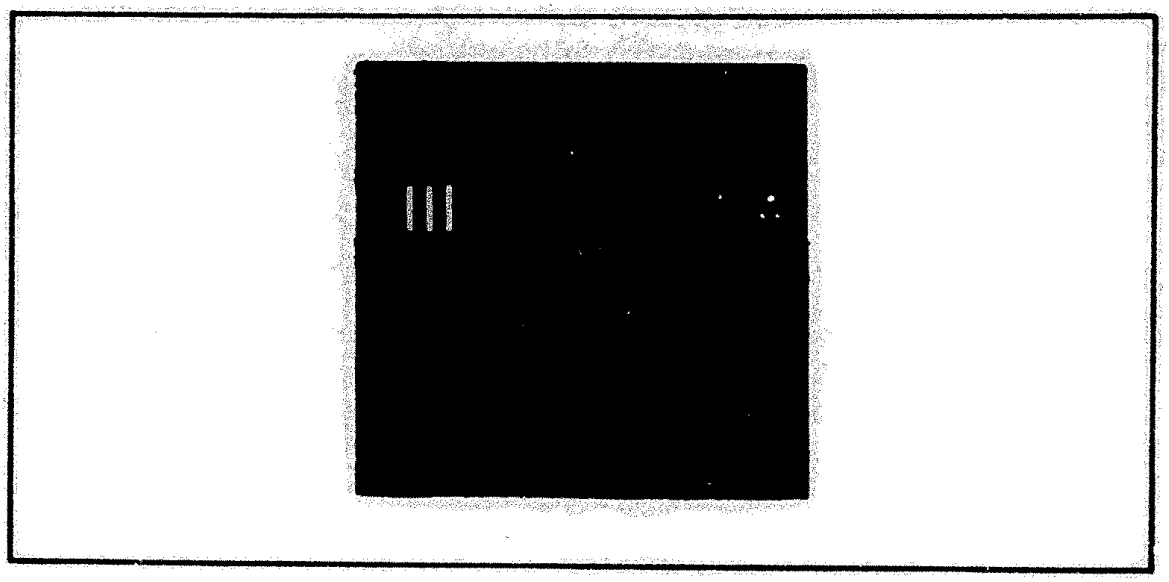

Fig. 78 Bar Patterns of Constant Aspect Used for Experiments

the isolated circles, an equivalent square is assumed, one whose area is the same as that of the circle, e.g.

$$x_o = \left(\frac{D^2}{4}\right)^{\frac{1}{2}} , \tag{157}$$

where D is the diameter of the circle.

For bar patterns, SNR_{DI} is calculated on the basis of the total area of a bar. Specifically, the equation

$$SNR_{DI} = \left[\frac{2t\, n_v\, \Delta f_V}{a}\right]^{\frac{1}{2}} \frac{R_{SF}(N)}{N\xi_y^{\frac{1}{2}}} \left(\frac{\Delta i}{I_n}\right) , \tag{158}$$

is used. In the above, Δi is the peak-to-peak signal current for a broad area pattern (unity modulation transfer function) and I_n is the rms noise that is added to the camera generated image. Real cameras, of course,

Pattern							
Isolated Circles		Isolated Bars		Variable Aspect Bar Patterns		Constant Aspect Bar Patterns	
N	n_v	N	n_v	N	n_v	N	n_v
37	1	74	5.3	74	5.3	104	5
71	1	261	19.0	261	19.0	200	5
121	1	357	25.8	357	25.8	329	5
184	1	494	35.6	494	35.6	396	5
300	1	625	45.1	625	45.1	482	5
314	1	760	54.8	760	54.8	635	5
866	1	900	65.0	900	65.0	729	5
		1090	78.6	1090	78.6	800	5
		1205	88.6	1205	88.6		
		1605	116.0	1605	116.0		
		1780	125.0	1780	125.0		

Table 9 Line Number and Bar Aspect for Various Patterns

have a response that is a function of frequency and the value of Δi in the video channel for square wave inputs becomes Δi_{p-p}, the peak-to-peak value of the video signal when the frequency effects are included. That is,

$$\Delta i_{p-p} = \Delta i \, R_{SQ}(N), \tag{159}$$

and

$$SNR_{DI} = \left[\frac{2t\, n_v\, \Delta f_V}{\alpha}\right]^{\frac{1}{2}} \left(\frac{1}{N}\right) \frac{R_{SF}(N)}{R_{SQ}(N)\xi_y^{\frac{1}{2}}} \frac{\Delta i_{p-p}}{I_N}, \tag{160}$$

where $R_{SF}(N)$ is the value of the flux factor at N, $R_{SQ}(N)$ is the value of the square wave response at N and Δi_{p-p} the value of the peak-to-peak signal corresponding to N as measured in the output of the video channel. Alternately, one could measure Δi for a broad area pattern and use Eq. (158).

In any event, ξ_y is given by

$$\xi_y = \left[1 + \left(\frac{N}{n_v N_{eL}}\right)^2 + \left(\frac{N}{n_v N_{eT}}\right)^2\right]^{\frac{1}{2}} \tag{161}$$

where

$$N_{eL} = \int \left|R_{oL}(N)\right|^2 dN \tag{162}$$

and

$$N_{eT} = \int \left|R_{oT}(N)\right|^2 dN \tag{163}$$

For calculation purposes, t, the integration time of the eye is taken to be 0.1 sec and α, the picture aspect ratio is 4/3. At low spatial frequencies the displayed images approach a square wave while at high spatial frequencies, above about 300 lines/picture height for Case A the

displayed images were nearly pure sine waves.

For the isolated bars and circles, the aperiodic object form of the signal-to-noise ratio should be used for calculating SNR_{DI} and it is repeated here as

$$SNR_{DI} = \left(\frac{2n_v t \ \Delta f}{\alpha}\right)^{\frac{1}{2}} \frac{1}{\xi_{xy}^{\frac{1}{2}}} \ \frac{1}{N} \ \frac{\Delta i}{I_n} \tag{164}$$

where

$$\xi_{xy} = \left[1 + \left(\frac{N}{N_{eI}}\right)^2 + \left(\frac{N}{N_{eT}}\right)^2\right]^{\frac{1}{2}} \cdot \left[1 + \left(\frac{N}{n_v N_{eL}}\right)^2 + \left(\frac{N}{n_v N_{eT}}\right)^2\right]^{\frac{1}{2}} \tag{165}$$

For the first experiment (called experiment #1), the constant aspect bar patterns were used. The experimental conditions were the same as those used previously (10 months earlier) which were reported in AFAL-TR-72-229 and the purpose of the present experiment was to establish a "bench mark" between the previous and the new results. Experimental conditions are listed in Table 10. Five subjects participated. In Fig. 79, the data from the present experiment is shown by the open circle points, o, and the original data by the solid circle points, •. A comparison of the two shows that there is nearly a constant percentage reduction in the threshold SNR_{DI} at a given line number for the new data. This difference was quite unexpected. In the original and the present experiment, the brightness of the room surrounding the monitor was approximately the same, .05 ft.Lambert.

The experiment was repeated with the same subjects with the room brightness surrounding the monitor equal to 1 ft. Lambert and the data is plotted in Fig. 80 with the threshold SNR_{DI} values plotted in Fig. 79 by

Exp. No.	Test Images	(1) L_O	(2) L_B	(3) MTF Shape	(4) No. Obs.	(5) No. of Trials	(6) No. of Scan Lines	(7) Frames/ Second	Figure No.
1	Constant Aspect	1	0.05	A	1	210	875	25	79
2	Constant Aspect	1	1	A	5	1230	875	25	80,88
3	Constant Aspect-Critical	1	1	A	1	217	875	25	81
4	Electronic Squares	1	0.05	A	4	720	525	30	82,83
5	Constant Aspect	1	1	B	5	1080	875	25	84,85 88
6	Constant Aspect	1	1	C	5	953	875	25	86,87 88
7	Constant Length	1	1	A	6	1730	875	25	89,91
8	Constant Length	1	1	C	5	1400	875	25	91
9	Isolated Bars	1	1	A	6	1730	875	25	92
10	Isolated Bars	1	1	C	5	1400	875	25	92
11	Isolated Circles	1	1	A	6	1730	875	25	93
12	Isolated Circles	1	1	C	5	1400	875	25	93
13	Tactical Targets	1	1	A	5	1000	875	25	93,94 95
14	Tactical Targets	1	1	C	5	1000	875	25	93
15	Tactical 10 Sec/PW	1	1	D	3	600	875	25	--

Table 10 Experimental Conditions

NOTES:

(1) Average Monitor Luminance, ft-L

(2) Average Background Luminance, ft-L

(3) MTF Case A, B, or C Used

(4) Total Number of Observers

(5) Total Number of Trials

(6) Number of Scan Lines per Picture Height, Interlaced

(7) Number of Frames per Second Noise Bandwidth 12.5 MHz, Viewing Distance 28 inches, 8-inch High Monitor